Publication Year	2018
Acceptance in OA	2020-11-24T14:12:58Z
Title	Revealing the Broad Line Region of NGC 1275: The Relationship to Jet Power
Authors	Punsly, Brian, MARZIANI, Paola, Bennert, Vardha N., Nagai, Hiroshi, Gurwell, Mark A.
Publisher's version (DOI)	10.3847/1538-4357/aaec75
Handle	http://hdl.handle.net/20.500.12386/28506
Journal	THE ASTROPHYSICAL JOURNAL
Volume	869

Revealing the Broad Line Region of NGC 1275: The Relationship to Jet Power

Brian Punsly[1], Paola Marziani[2], Vardha N. Bennert[3], Hiroshi Nagai[4,5] and Mark A. Gurwell[6]

ABSTRACT

NGC 1275 is one of the most conspicuous active galactic nuclei (AGN) in the local Universe. The radio jet currently emits a flux density of ~ 10 Jy at ~ 1 mm wavelengths, down from the historic high of ~ 65 Jy in 1980. Yet, the nature of the AGN in NGC 1275 is still controversial. It has been debated whether this is a broad emission line (BEL) Seyfert galaxy, an obscured Seyfert galaxy, a narrow line radio galaxy or a BL-Lac object. We clearly demonstrate a persistent Hβ BEL over the last 35 years with a full width half maximum (FWHM) of 4150 - 6000 km/s. We also find a prominent Pα BEL (FWHM ≈ 4770 km/s) and a weak CIV BEL (FWHM ≈ 4000 km/s), Hβ/CIV ≈ 2. A far UV HST observation during suppressed jet activity reveals a low luminosity continuum. The Hβ BEL luminosity is typical of broad line Seyfert galaxies with similar far UV luminosity. X-ray observations indicate a softer ionizing continuum than expected for a broad line Seyfert galaxy with similar far UV luminosity. This is opposite of the expectation of advection dominated accretion. The AGN continuum appears to be thermal emission from a low luminosity, optically thick, accretion flow with a low Eddington ratio, ~ 0.0001. The soft, weak ionizing continuum is consistent with the relatively weak CIV BEL. Evidence that the BEL luminosity is correlated with the jet mm wave luminosity is presented. Apparently, the accretion rate regulates jet power.

---

[1] 1415 Granvia Altamira, Palos Verdes Estates CA, USA 90274: ICRANet, Piazza della Repubblica 10 Pescara 65100, Italy and ICRA, Physics Department, University La Sapienza, Roma, Italy, brian.punsly@cox.net

[2] INAF, Osservatorio Astronomico di Padova, Italia

[3] Physics Department, California Polytechnic State University, San Luis Obispo, CA 93407, USA

[4] National Astronomical Observatory of Japan, Osawa 2-21-1, Mitaka, Tokyo 181-8588, Japan

[5] The Graduate University for Advanced Studies (SOUKENDAI), Osawa 2-21-1, Mitaka, Tokyo 181-8588, Japan

[6] Harvard-Smithsonian Center for Astrophysics, Cambridge, MA USA

Subject headings: black hole physics — galaxies: jets—galaxies: active — accretion, accretion disks

1. Introduction

The galaxy NGC 1275 was distinguished from other extragalactic objects as an active galactic nucleus (AGN) due to its bright stellar like nucleus and strong emission lines (Humason 1932; Seyfert 1943). It lies at the heart of the Perseus cluster of galaxies. It has been the brightest extragalactic radio source (3C 84) at high frequency with flux densities of 45Jy - 65Jy in 1980 at 270 GHz and $\sim 40-50$ Jy at 90 GHz from 1965-1985 (Nesterov et al. 1995). The large radio flare began in the 1950s and was accompanied by large optical flares in the 1970s (Nesterov et al. 1995). The flare subsided in the 1990s, but a new strong flare began in 2005. The physical nature of the AGN is of great interest due to the powerful radio jet and its relationship to the feedback in the cluster cooling flow.

In spite of its proximity ($z = 0.0175$) and unique properties, the nature of the AGN has been the subject of controversy within standard classification schemes that are designed to segregate physical characteristics. In the original classification scheme, it was considered a Seyfert 2 galaxy (Khachikian and Weedman 1969; Chuvaev 1985). Noting the wildly varying optical flux, it was later called a BL-Lac object (Veron 1978). Reports of a weak broad emission line (BEL) region based on Hα were later made with better spectra and a classification of Seyfert 1.5 was assigned (Filippenko and Sargent 1985; Ho et al. 1997). However, BELs were not detected by other observers with the same telescope, but they did conclude that it could not be ruled out due to insufficient signal to noise (Rosenblatt et al. 1994). More recently, the general notion of identifying emission lines as weak BELs as opposed to wide narrow lines (NLs) in AGN has been the subject of controversy. To resolve the issue, narrow (0.1"-0.2") slit HST observations of many of the radio galaxies in Ho et al. (1997) were performed. The small aperture excludes much of the Hα NL emission. This showed that many of these radio galaxies did not have a BEL in Hα (Balmaverde and Capetti 2014). Thus, NGC 1275 is often called a NL radio galaxy. Even so, its classification as a low or high excitation radio galaxy (i.e., does it have a strong photo-ionization source in the accretion flow?) is controversial (Buttiglione et al. 2010; Son et al. 2012). From a physical point of view, these distinctions are critical. Is the powerful radio jet ejected from a hot advection dominated accretion flow (ADAF), Narayan and Yi (1994), or does it emanate from an accretion flow that cools by thermal emission from optically thick gas (that photo-ionizes the surrounding gas)?

Thus motivated, we look for evidence of the BEL in high signal to noise spectra both

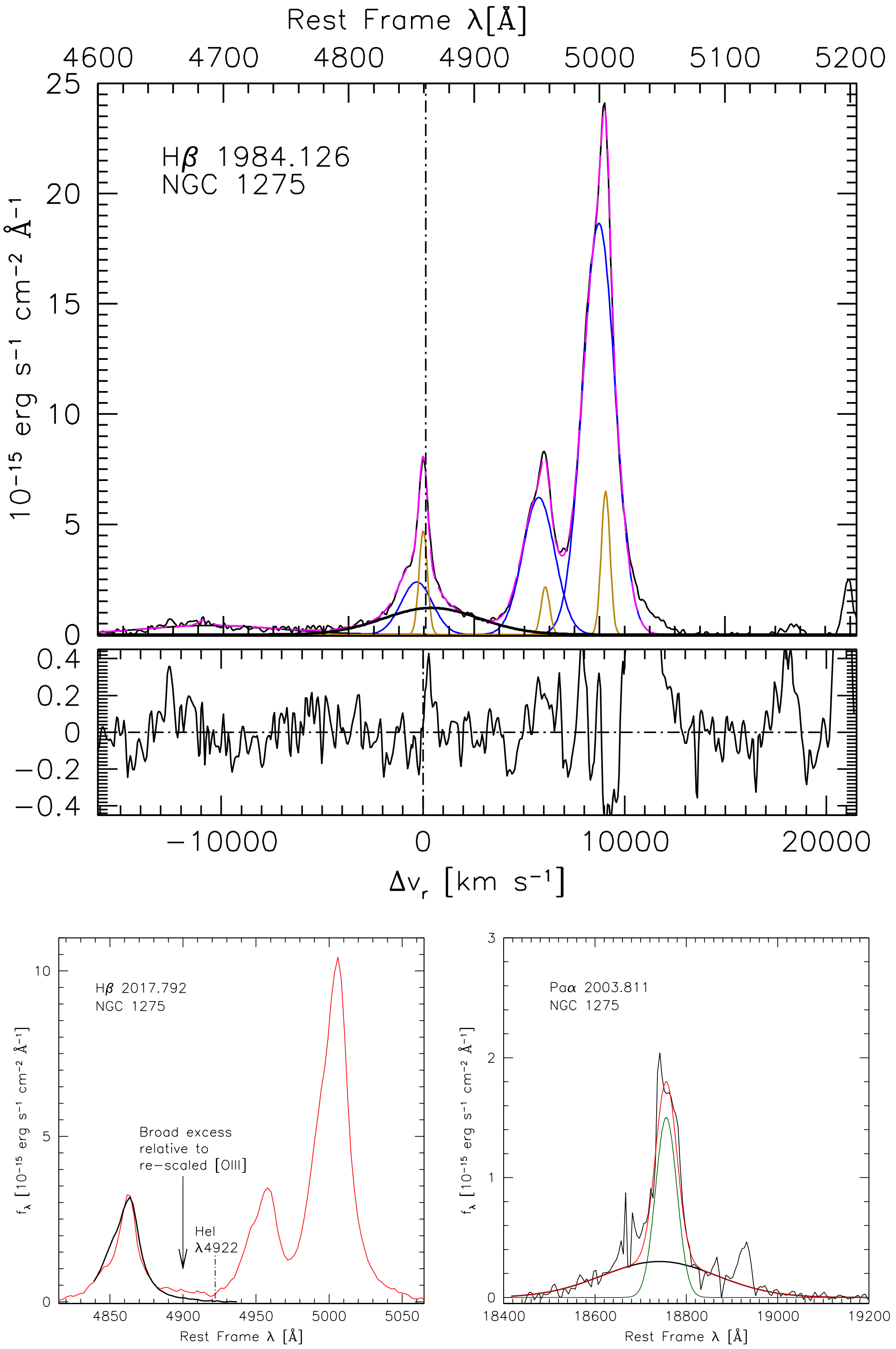

Fig. 1.— The top frame illustrates our fitting procedure for the Hβ and [OIII] complex (epoch 1984.126) that is described in the text. The BEL, semi-broad NL, and NL (wind) are black, blue and yellow, respectively. The bottom left frame shows the redwing excess of Hβ relative to a scaled [OIII] NL profile. Note that there is no evidence of a weak HeI λ4922 emission line or the FeII λ4924 emission line. The bottom right frame shows the BEL (NNL) in Pα in brown (green).

historical and with new spectral observations. We concentrate on $H\beta$ rather than $H\alpha$ even though it is considerably weaker and potentially suffers from FeII contamination. These issues are less severe than subtracting [NII] from the $H\alpha$ + [NII] complex. Subtracting [NII] from the composite profile using other strong NL profiles is nontrivial and is highly dependent on the NL profile ([SII] or [OI]) that is utilized to scale the subtraction (Balmaverde and Capetti 2014). In Section 2 and 3, we describe the BELs. Section 4 is a discussion of the ionizing continuum and the Section 5 describes the BEL - jet connection.

2. Simultaneous Fits of Hβ and [OIII]$\lambda\lambda$4959, 5007

In this analysis, it is very important to fit self-consistently Hβ and [OIII]$\lambda\lambda$4959, 5007. The models were carried out assuming two NL components: a semi broad NL and a narrower NL (perhaps of galactic wind origin or unperturbed bulge gas) for both [OIII] and Hβ. For the [OIII] doublet, we adopt the usual condition that the 4959 $\AA$ line flux is 1/3 of the 5007 $\AA$ line flux and the two components have the same velocity and FWHM (Dimitrijević et al. 2007). The same velocity and FWHM were applied to the corresponding two NL components of Hβ. The FeII subtraction is accomplished using an FeII template based on I Zw 1, see Marziani et al. (2009), Section 2.3. The FeIIλ4570 blend is undetectable (Boroson and Green 1992). Thus, the template indicates that FeIIλ4924 is very weak and won't affect our fit (see Figure 1). For the sake of scientific rigor all the data need to be fit with the same methodology. Previously published results are refit.

Table 1 describes the line fits with complete expository text and labels. All of the data is archival except for our new observation in 2017. Long slit spectra were obtained with the AFOSC camera mounted at the Cassegrain focus of the Copernico telescope on Mount Ekar, on Oct. 18, 2017 and Oct. 26, 2017 (Grism # 7). The slit was opened to 1.69", and 2.50" at parallactic PA and at PA=90, and spectra were extracted as reported in Table 1. The GR # 7 yields an inverse resolution of $\approx$ 590 for a slit width 1.69", allowing for an effective deblending of the BC from the wind and narrow components. The 2D frames of the spectra were bias subtracted, flat fielded, wavelength and flux calibrated. The wavelength calibration obtained from lamps of Th and Ar was realigned on the sky lines of the source frame, yielding a dispersion in residual sky line shifts with respect to rest wavelength of 0 ± 25 km/s. The flux calibration was achieved by the observations of tertiary standard stars obtained with the same slit width right before and after NGC 1275. The adopted absolute flux scale at fixed aperture is believed to be accurate to about 10% at a 1σ confidence level.

The top frame of Figure 1 shows the fit to the strongest Hβ BEL. The BEL is not obvious because it does not dominate the NL contribution to the combined profile. The bottom two frames in Figure 1 corroborate the BEL identification. For illustrative purposes, the bottom left frame shows the residual excess in the redwing that occurs if one tries to fit Hβ with NLs only. If we simply re-scale the amplitude of [OIII]λ5007 and then center it on Hβ, the figure shows a " red shelf" of excess flux. Mathematically, we performed an F-test between the best fit with and without a BEL. For 641 degrees of freedom, the F-statistic was 2.768 which implies a better fit with the BEL at $> 99.999\%$ significance level. The result derives primarily from residuals below the "red shelf". The bottom right hand frame shows the Pα line which also arises from transitions from the n=4 state. There is a clear BEL with a similar FWHM to the Hβ BELs in Table 1, 4770 km/s.

The line luminosity in Table 1 was computed using the following cosmological parameters: H_0=71 km/s/Mpc, $\Omega_\Lambda = 0.73$ and $\Omega_m = 0.27$ and $z = 0.0175$. Notice that we fit [OII]λ3727 as well as CIV and Pα. Line luminosity is corrected for Galactic extinction. The best fit to the extinction values in the NASA Extragalactic Database (NED) in terms of Cardelli et al. (1989) models is $A_V = 0.438$ and $R_V = 3.0$.

Table 1: NGC 1275 Emission Line Fits

		Optical			Emission			Lines			
1	2	3	4	5	6	7	8	9	10	11	12
Date	Extraction Region Arcsec	$H\beta$ (broad) Luminosity ergs/s	$H\beta$ (broad) FWHM km/s	[OIII] (NL)[a] Luminosity ergs/s	[OIII] (NL)[a] FWHM km/s	[OIII] galactic)[a] Luminosity ergs/s	[OIII] (galactic)[a] FWHM km/s	$H\beta$ (NL) Luminosity ergs/s	$H\beta$ (galactic) Luminosity ergs/s	[OII] Luminosity ergs/s	Reference
1983.940[b]	2 x 128[c]	1.28×10^{41}	5161 ± 33	6.20×10^{41}	1825 ± 5	2.32×10^{40}	482	6.27×10^{40}	3.96×10^{40}	2.49×10^{41}	Lawrence et al. (1996)
1984.126[b]	2 x 4[c]	1.28×10^{41}	5536 ± 196	6.52×10^{41}	1821 ± 6	6.06×10^{40}	484	8.32×10^{40}	4.33×10^{40}	...	Ho et al. (1995)
1994.940[e]	≈2.6 x 3[c]	7.88×10^{40}	5162 ± 275	5.05×10^{41}	1754 ± 7	6.57×10^{40}	588	5.70×10^{40}	4.46×10^{40}	3.55×10^{41}	Marziani et al. (1996)
2000.663[f]	0.2 x 0.2	6.10×10^{40}	4169 ± 299	3.81×10^{41}	1907 ± 17	5.42×10^{38}	897	4.99×10^{40}	1.44×10^{40}	8.40×10^{40}	This paper
2008.016[g,h]	2 x 2 [d]	9.21×10^{40}	4260 ± 138	3.62×10^{41}	2046 ± 23	5.73×10^{40}[h]	1115	2.66×10^{40}[h]	4.11×10^{40}[h]	2.42×10^{41}	Buttiglione et al. (2009)
2009.646[i]	2 x 2 [d]	8.77×10^{40}	4556 ± 75	3.67×10^{41}	1774 ± 5	5.77×10^{40}	560	4.45×10^{40}	3.42×10^{40}	2.00×10^{41}	Son et al. (2012)
2009.646[i]	2 x 3 [d]	9.66×10^{40}	4475 ± 77	4.32×10^{41}	1768 ± 5	7.03×10^{40}	551	5.12×10^{40}	4.08×10^{40}	2.41×10^{41}	Son et al. (2012)
2009.646[i]	2 x 4 [d]	9.41×10^{40}	4470 ± 87	4.60×10^{41}	1764 ± 5	7.94×10^{40}	542	5.84×10^{40}	4.37×10^{40}	2.66×10^{41}	Son et al. (2012)
2017.792[j]	1.69 x 2 [d]	8.18×10^{40}	5973 ± 322	2.92×10^{41}	1779 ± 17	4.76×10^{40}	590	3.66×10^{40}	2.93×10^{40}	...	This paper
2017.792[j]	2.5 x 2.5 [d]	7.81×10^{40}	4667 ± 137	3.92×10^{41}	1809 ± 7	3.93×10^{40}	710	4.88×10^{40}	3.91×10^{40}	...	This paper
2017.792[j]	2.5 x 2.5[c]	1.05×10^{41}	4967 ± 106	4.14×10^{41}	1805 ± 7	7.26×10^{40}	690	4.88×10^{40}	4.52×10^{40}	...	This paper
2017.792[j]	2.5 x 3.5[c]	9.28×10^{40}	4395 ± 184	4.65×10^{41}	1786 ± 9	8.45×10^{40}	678	5.86×10^{40}	4.88×10^{40}	...	This paper

		Other			Emission			Lines			
1	2	3	4	5	6	7	8	9	10	11	12
Date	Extraction Region Arcsec	$P\alpha$ (broad) Luminosity ergs/s	$P\alpha$ (broad) FWHM km/s	$P\alpha$ (NL) Luminosity ergs/s	$P\alpha$ (NL) FWHM km/s	CIV (broad) Luminosity ergs/s	CIV (broad) FWHM km/s	CIV (NL) Luminosity ergs/s	CIV (NL) FWHM km/s	HeII (broad) Luminosity ergs/s	Reference
2003.811[k]	0.8" x 15"	6.56×10^{40}	4770 ± 200	6.12×10^{41}	880 ± 175	...	...	...	...	...	Riffel et al. (2006)
1993.093[l]	0.25" x 1.23"	...	...	...	...	3.39×10^{40}	4297 ± 974	5.09×10^{40}	1629 ± 40	...	Marziani et al. (1996)
2011.352[m]	2" x 2"	...	...	...	...	4.22×10^{40}	4477 ± 933	6.82×10^{40}	1431 ± 70	3.14×10^{40}	This paper

---

[a] $\lambda = 5007$, total luminosity of doublet is found by multiplying by 1.33. NL is the narrow line associated with the AGN and galactic is large scale galactic gas emission

[b] Hale Telescope

[c] Slit along PA = 90 degrees

[d] Slit at parallactic angle

[e] San Pedro Martir 2.2 Meter

[f] HST STIS G430L

[g] Telescopio Nazionale Galileo, 3.58 meter

[h] ow resolution, 20Å: characterizations of NLs not accurate and FWHMs not accurate especially for NLs

[i] ick 3 meter

[j] Copernico Telescope, 1.8 Meter. The observations were performed for the purposes of this study

[k] NASA 3m Infrared Telescope Facility

[l] HST FOS G130H

[m] HST COS G160M. Guide star acquisition failed. Thus, CIV luminosity possibly underestimated due to slit losses from poor centering late in the observation.

It is important to note that the observations in Table 1 were not preferentially selected because they showed a BEL. These were all the available data-sets that could be obtained from data archives or through direct contact with principal investigators. We know of no other data that is well calibrated with good signal to noise for which the data was available. For all the observations in Table 1, the addition of a broad component improved the fit because of the issue of the excess illustrated by the lower left hand frame of Figure 1 and the related discussion.

Table 1 contains two important experiments based on the 2009 and 2017 data. Different extraction regions were applied to the data and in 2017 different slit orientations were tried. The 2017 experiment indicates that the Hβ BEL fits were not driven by slit angle or extraction region as long as the extraction region was larger than the dimensions set by "seeing". Thus, the values in Table 1 are robust for comparing the time evolution of the Hβ BEL. Conversely, the NL luminosity scales with the size of the extraction region.

3. The CIV Broad Emission Line

The top frame of Figure 2 shows that a NL cannot fit the 2011 CIV emission line. There is a significant excess in the red wing and a smaller excess in the blue wing that cannot be removed by raising the continuum level. The bottom frame shows fits to two epochs obtained by adding a BEL. The BEL+NL model fits are not well constrained by the noisy data and the data gap in 2011. We remove some arbitrariness by requiring that the NL FWHM agree to within 15% between the two epochs. The results are shown in Table 1 and Figure 2. In spite of the aforementioned data quality, it is apparent that the BEL is extremely weak, even compared to the weak $H\beta$ BELs. Based on Table 2, the ratio of BEL luminosity L(CIV)/L($H\beta$) $\approx$ 1/2. We compare this to other "Population B" AGN defined by a FWHM of $H\beta$ that exceeds 4000 km/sec, as is the case for NGC 1275 (Sulentic et al. 2000). For Population B AGN, typically, L(CIV)/L($H\beta$) $\approx$ 5-7 (Sulentic et al. 2007).

4. The Nature of the Accretion Flow

The cause of the weak BELs and CIV in particular are a major diagnostic of the central AGN. The weak BEL can arise from

1. a lack of BEL gas
2. intrinsic extinction

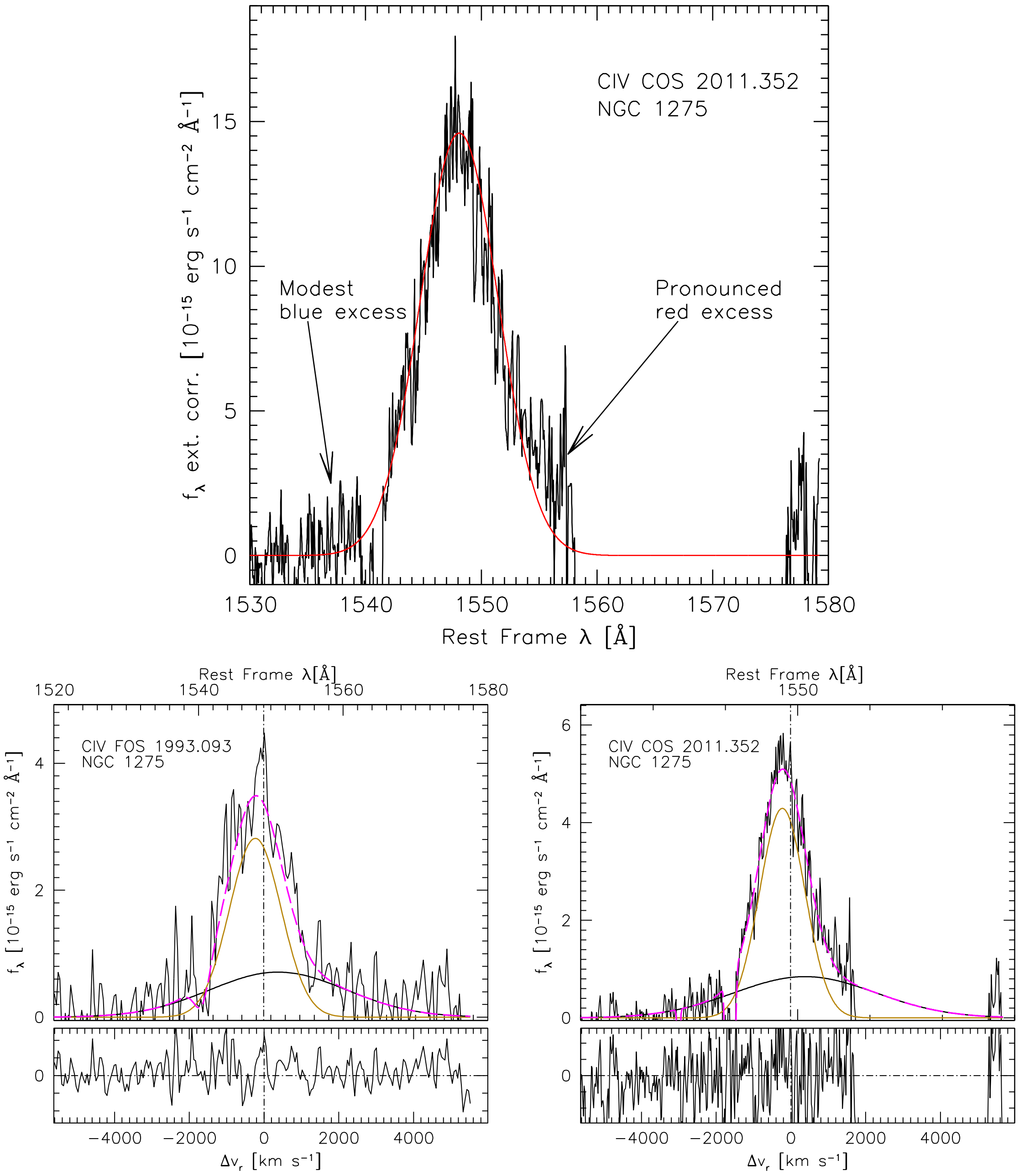

Fig. 2.— The top frame illustrates that the widest plausible NL fit to CIV in 2011.352 still results in a significant redwing residual. The bottom frame fits the CIV profile with a NL+BEL in 1993.093 (left) and 2011.352 (right).

3. a weak ionizing continuum

This section synthesizes broad band data and CLOUDY simulations in order to discriminate between these three possibilities.

4.1. The Ionizing Continuum

In order to analyze these alternatives, we constrain the accretion flow properties. This is difficult because the accretion flow is under-luminous and is typically dominated in the optical band by the high frequency synchrotron tail of the jet emission. The best chance of finding the signature of the accretion flow is to look at high frequency, where synchrotron cooling tends to lower the luminosity, most importantly in a very low state. The 1993 HST FOS far UV observation in Table 1 fits these criteria. The narrow slit is advantageous for reducing background flux, but requires a careful observation to avoid centering losses. There is an estimated centering offset of 0.034" from the acquisition procedure (Evans et al. 2004). Thus, we do not expect centering losses to affect the absolute flux calibration. The spectral index of the continuum, after Galactic de-reddening, $\alpha_{\lambda} \approx -1.5$ ($F_{\lambda} \sim \lambda^{\alpha_{\lambda}}$), is typical of the far UV continuum ($1100\mathring{A} < \lambda < 1600\mathring{A}$) in low redshift, low luminosity type 1 AGN based on HST spectra (Stevans et al. 2014). The spectral energy is $\lambda L_{\lambda}(1450\mathring{A}) = 3.5 \times 10^{42}$ergs/s. These numbers suggest a comparison to low luminosity broad line Seyfert galaxies. Fortunately, there are low luminosity Seyfert galaxies in the broad line reverberation sample. The reverberation study of Kaspi et al. (2005) has a wealth of broadband data (i.e., far UV, X-ray and Hβ BEL luminosity). This sample covers a large range of far UV luminosity that photo-ionizes the BEL in the reverberation methodology. In order to ensure that we are comparing to potentially similar objects, we choose a "control" subsample defined by an upper limit $\lambda L_{\lambda}(1450\mathring{A}) < 10^{44}$ergs/s, i.e. ~ 30 times stronger than 3C 84, in order to study the nature of the ionizing continuum.

Figure 3 characterizes 3C 84 in the context of the Kaspi et al. (2005) control sample. The left hand side plots the Hβ BEL luminosity, $L(H\beta)$, versus the far UV luminosity, $\lambda L_{\lambda}(1450\mathring{A})$. This is a good surrogate for the soft ionizing continuum at $\lambda < 900\mathring{A}$. We added NGC 1275 to the scatter plot by using the 1994 $L(H\beta)$ in Table 1, since it is closest in time to the far UV observation. The left hand frame indicates that $L(H\beta)/\lambda L_{\lambda}(1450\mathring{A})$ is typical of what one expects for a low luminosity broad line Seyfert galaxy. $L(H\beta)$ trends with $\lambda L_{\lambda}(1450\mathring{A})$ in Figure 3, indicating that a weak photo-ionizing continuum is responsible for the small $L(H\beta)$ for both the Kaspi et al. (2005) control sample and NGC 1275. NGC 1275 is not an outlier in the $L(H\beta)$-$\lambda L_{\lambda}(1450\mathring{A})$ scatter plane contrary to the expectation that the weak BEL is a consequence of a paucity of BEL gas relative to the control sample (condition 1, above).

Next, we try to assess the hard ionizing continuum by looking at the X-ray luminosity between 2 and 10 keV, L_{2-10}. The X-ray luminosity of the accretion flow is not known, but there are some useful upper limits. Chandra observations in 2002 are used to estimate L_{2-10} within $\sim$ 1.2" of the nucleus (Balmaverde et al. 2006). A short, off-axis, observation, $\sim$5 ks, that had a very low count rate compared to other observations before 2006, 21 cts/s, was utilized in order to minimize the effects of pile-up associated with the nucleus. The spectrum is unabsorbed, and is likely primarily of jet origin which consistently has a mm band luminosity $> 10^{43}$ergs/s and a gamma-ray luminosity $\sim 10^{44}$ergs/s (Abdo et al. 2010). Thus, this is a very loose upper bound on L_{2-10} from the accretion flow in the right hand frame of Figure 3. Another method of estimating L_{2-10} from accretion is to look for an absorbed component of X-ray flux. This has been done based on XMM data (Hardcastle et al. 2009). Their result is shown as an upper bound in the right hand frame of Figure 3. This figure indicates that $L_{2-10}/\lambda L_{\lambda}(1450\AA)$ is much less than would be expected for a low luminosity broad line Seyfert galaxy and contrary to the basic prediction of an ADAF (Mahadevan 1997).

In summary, the two panels of Figure 3 and $\alpha_{\lambda} \approx -1.5$ in the far UV seem to indicate a broad line Seyfert-like AGN with a typical soft ionizing continuum and a weak hard ionizing continuum. Broad line Seyfert-like AGN are believed to be a consequence of thermal emission from optically thick, geometrically thin accretion (Sun and Malkan 1989).

Not only is the ionizing continuum weak based on $R_{\rm Edd}$, but it is also soft. Both factors would conspire to make the recombination rate fast relative to the photo-ionization rate. Thus, less cooling occurs through high ionization state atomic transitions. The weak ionizing continuum of 3C 84 is a viable explanation of the low CIV/Hβ BEL luminosity ratio. Even though the BEL region is complicated by stratification and anisotropy, simulations of individual clouds routinely show that $L(CIV)$ decreases faster than $L(H\beta)$ as the ionizing continuum becomes more dilute (Korista et al. 1997).

4.2. CLOUDY Simulations

Table 1 provides some very strong constraints of the BEL region. If we take into account, the uncertainty in our estimates and some possible modest intrinsic extinction that affects the UV more than the optical, we have the following BEL constraints,

$$\frac{L(CIV)}{L(H\beta)} = 0.3\text{--}0.8 \ , \ \frac{L(P\alpha)}{L(H\beta)} = 0.6\text{--}1.1 \ , \ \frac{L(FeII)}{L(H\beta)} < 0.3 \ , \ \frac{L(HeII\lambda1640)}{L(CIV)} = 0.5\text{--}1.0 \ . \quad (1)$$

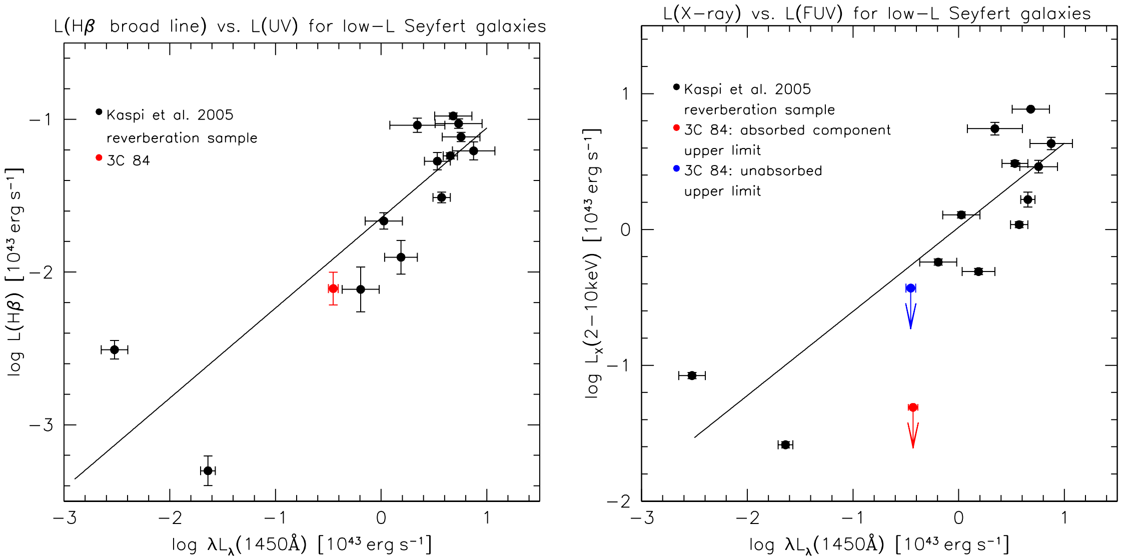

Fig. 3.— Diagnostics of the photo-ionizing continuum. The left frame shows that 3C 84 has a far UV-Hβ ratio similar to that of weak broad line Seyfert galaxies. The right frame indicates that the ionizing continuum is softer than a typical broad line Seyfert galaxy of similar far UV luminosity. The unabsorbed Chandra estimate is a very loose upper bound as discussed in the text. The lines are the best fit power laws to the Kaspi et al. (2005) data.

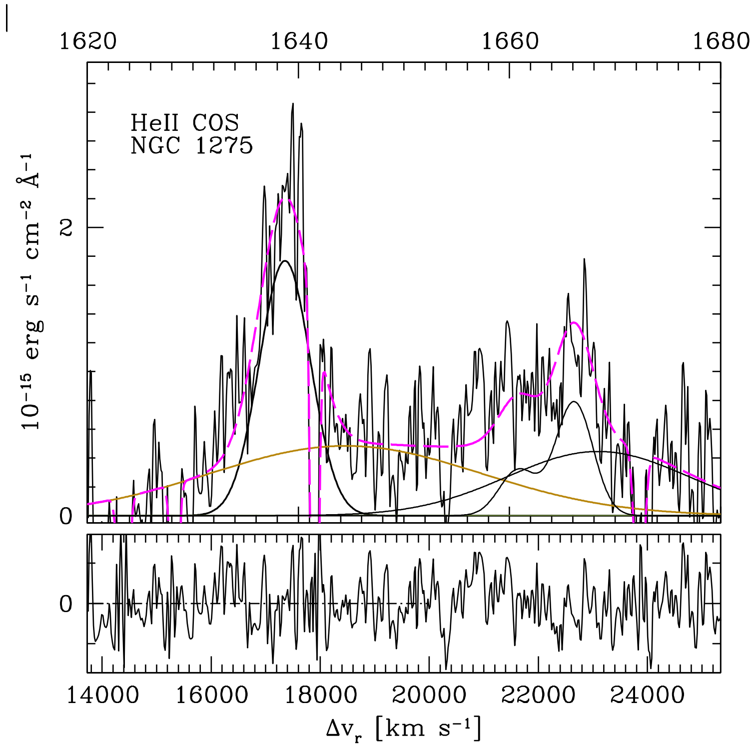

Fig. 4.— Low ionization parameter simulations predict a strong HeIIλ1640 BEL relative to the nearby CIV BEL. The fit is fairly complicated. There are narrow and broad (brown) HeII lines and a broad AlIIλ1671 line. In addition there are the two NLs OIII]λ 1666 and OIII]λ1663 that are fit in a 2.5:1 ratio. The estimate of the HeII BEL line strength is recorded in Table 1.

The details of the HeII fit to the 2003 COS data are shown in Figure 4. Note that the HeII/CIV ratio is unaffected by possible centering issues that were noted in the footnote to Table 1. We can use these ratios in order to explore the nature of the ionizing continuum and the nature of the BEL gas.

We performed CLOUDY 13 single zone models (see Table 2) in order to achieve a qualitative understanding of the constraints on the BEL and photo-ionizing continuum that are consistent with the observations of NGC 1275 (Ferland et al. 2013). Section 4.1 and Figure 3 describe our observed constraints on the photo-ionizing continuum. Our estimated photo-ionizing continuum has a spectral index $\alpha_\nu = 0.5$ (as observed in the far UV) from $5000\mathring{A}$ to $800\mathring{A}$. The spectral break point at $800\mathring{A}$ is fairly typical of other low luminosity Seyfert galaxies (Stevans et al. 2014). Beyond the spectral break, we choose $\alpha_\nu = 2$ down to the soft X-ray band at 0.5 keV. The spectral index is chosen to be $\alpha_\nu = 1.0$ in the X-ray band (see Figure 5). The results of our CLOUDY simulations are presented in Table 2. All the simulations have a similar L(Hβ) and a covering fraction of 1 in an open geometry in order to explore trends that are conducive to reproducing the observed line ratios. The ionization parameter, U, is the number density of ionizing photons for hydrogen (number density of photons with $\lambda < 912\mathring{A}$) divided by the hydrogen number density, n in column (2), in the single zone model. We identify two regions of parameter space that conform to the constraints imposed by observation. The first possibility is a very low ionization parameter $\log U \approx -2.5$ with solar metallicity ($Z = 1$) at large distances from the ionizing source, $\lesssim 10^{17}$cm. The other plausible region of parameter space has a slightly low ionization parameter $\log U \approx -1.5$ and a loosely constrained distance from the source, $3 \times 10^{16}\text{cm} - 10^{17}\text{cm}$, but requires a very low metallicity. The first alternative is what was expected based on the discussion at the end of Section 4.1.

These simulations show that the ionizing continuum of NGC 1275 is consistent with the unusual BEL line ratios and the low BEL luminosity. In particular, it explains the weak CIV BEL luminosity relative to the Hβ luminosity as well as the inordinately strong HeIIλ1640 BEL line strength relative to the CIV line strength.

In order to distinguish between the $Z = 0.1$ and $Z = 1.0$ solutions, we explore the Eddington ratio for more constraints on the system.

4.3. Eddington Ratio

The possibility of an optically thick thermal accretion flow is interesting considering the low luminosity. We assume the far UV power law extends from $10000\mathring{A}$ to as far down

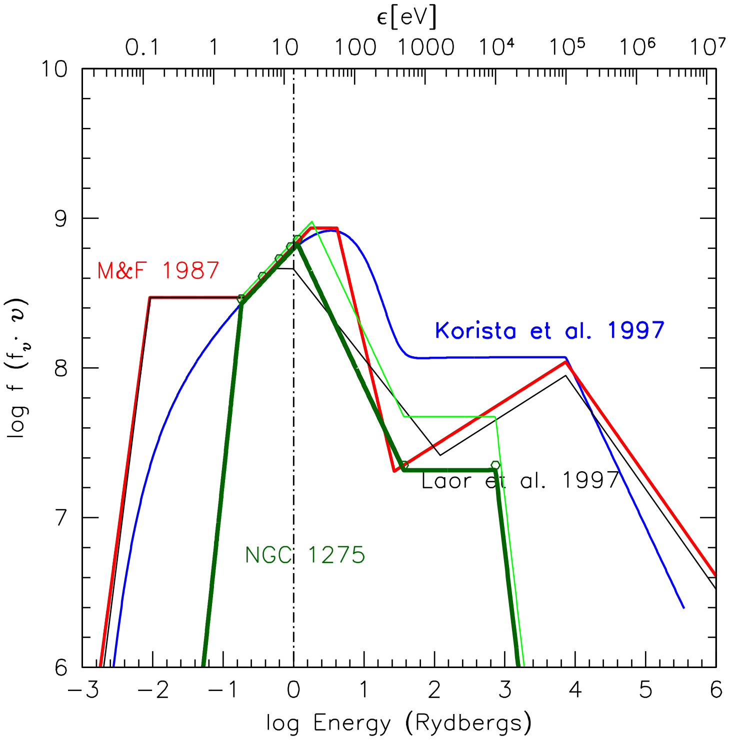

Fig. 5.— Comparison of the ionizing continuum inferred for NGC 1275 from the last subsection compared to other popular ionizing continua used in the literature as input spectra for CLOUDY simulations of AGN BELs (Mathews and Ferland 1987; Korista et al. 1997; Laor et al. 1997). The ionizing spectrum of NGC 1275 in green is softer.

Table 2: CLOUDY Simulations: NGC 1275

1	2	3	4	5	6	7	8	9	10	11
Z	$\log n$	$\log N_H$	$\log r$	$\log U$	$\log L(H\beta)$	CIV/$H\beta$	Pα/$H\beta$	HeII/CIV	FeII/$H\beta$	Conformance
Metalicity	Number Density cm−3	Column Density cm−2	Radius cm	Ionization Parameter	Luminosity erg/sec	Target 0.3 - 0.8	Target 0.6 - 1.1	Target 0.5 - 1.0	Target < 0.3	
0.1	9.75	22.7	16.5	-1.24	40.76	1.63	0.99	0.44	0.03	No
0.1	9.75	23.3	16.5	-1.24	40.80	1.47	1.09	0.43	0.06	No
0.1	9.75	22.7	16.75	-1.74	40.76	1.63	0.99	0.44	0.03	No
0.1	9.75	23.3	16.75	-1.74	40.80	1.47	1.09	0.43	0.06	No
0.1	9.75	22.7	17.0	-2.24	40.76	1.63	0.99	0.44	0.03	No
0.1	9.75	23.3	17.0	-2.24	40.80	1.47	1.09	0.43	0.06	No
0.1	10.0	22.7	16.5	-1.49	40.81	0.63	0.92	0.99	0.02	Yes
0.1	10.0	23.3	16.5	-1.49	40.84	0.59	1.01	0.97	0.05	Yes
0.1	10.0	22.7	16.75	-1.99	40.81	0.63	0.91	0.99	0.02	Yes
0.1	10.0	23.3	16.75	-1.99	40.84	0.59	1.01	0.97	0.05	Yes
0.1	10.0	22.7	17.0	-2.49	40.81	0.63	0.91	0.99	0.02	Yes
0.1	10.0	23.3	17.0	-2.49	40.84	0.59	1.01	0.97	0.05	Yes
0.1	10.25	22.7	16.5	-1.74	40.87	0.20	0.84	2.64	0.02	No
0.1	10.25	23.3	16.5	-1.74	40.89	0.19	0.93	2.59	0.04	No
0.1	10.25	22.7	16.75	-2.24	40.87	0.20	0.84	2.64	0.02	No
0.1	10.25	23.3	16.75	-2.24	40.89	0.19	0.93	2.59	0.04	No
0.1	10.25	22.7	17.0	-2.74	40.87	0.20	0.84	2.64	0.02	No
0.1	10.25	23.3	17.0	-2.74	40.89	0.19	0.93	2.59	0.04	No
0.1	10.5	22.7	16.5	-1.99	40.93	0.06	0.77	8.22	0.02	No
0.1	10.5	23.3	16.5	-1.99	40.94	0.05	0.87	8.08	0.03	No
0.1	10.5	22.7	16.75	-2.49	40.93	0.06	0.77	8.22	0.02	No
0.1	10.5	23.3	16.75	-2.49	40.94	0.05	0.87	8.08	0.03	No
0.1	10.5	22.7	17.0	-2.99	40.93	0.06	0.77	8.22	0.02	No
0.1	10.5	23.3	17.0	-2.99	40.94	0.05	0.87	8.08	0.03	No
1.0	9.75	22.7	16.5	-1.24	40.75	11.8	0.33	0.07	0.04	No
1.0	9.75	23.3	16.5	-1.24	40.83	9.77	0.35	0.07	0.07	No
1.0	9.75	22.7	16.75	-1.74	40.82	7.67	0.60	0.08	0.08	No
1.0	9.75	23.3	16.75	-1.74	40.89	6.49	0.54	0.08	0.11	No
1.0	9.75	22.7	17.0	-2.24	40.76	3.85	1.02	0.18	0.19	No
1.0	9.75	23.3	17.0	-2.24	40.78	3.65	1.05	0.18	0.27	No
1.0	10.0	22.7	16.5	-1.49	40.71	11.2	0.32	0.07	0.05	No
1.0	10.0	23.3	16.5	-1.49	40.77	9.72	0.36	0.07	0.08	No
1.0	10.0	22.7	16.75	-1.99	40.85	5.20	0.52	0.11	0.07	No
1.0	10.0	23.3	16.75	-1.99	40.88	4.84	0.56	0.11	0.11	No
1.0	10.0	22.7	17.0	-2.49	40.79	1.91	0.97	0.32	0.22	No
1.0	10.0	23.3	17.0	-2.49	40.81	1.84	1.00	0.32	0.22	No
1.0	10.25	22.7	16.5	-1.74	40.69	9.33	0.35	0.09	0.06	No
1.0	10.25	23.3	16.5	-1.74	40.73	8.40	0.34	0.09	0.09	No
1.0	10.25	22.7	16.75	-2.24	40.81	3.55	0.55	0.17	0.08	No
1.0	10.25	23.3	16.75	-2.24	40.86	3.15	0.54	0.17	0.11	No
1.0	10.25	22.7	17.0	-2.74	40.83	0.76	0.91	0.73	0.12	Yes
1.0	10.25	23.3	17.0	-2.74	40.85	0.73	0.94	0.73	0.18	Yes
1.0	10.5	22.7	16.5	-1.99	40.66	7.09	0.34	0.13	0.07	No
1.0	10.5	23.3	16.5	-1.99	40.68	6.86	0.41	0.13	0.11	No
1.0	10.5	22.7	16.75	-2.49	40.82	1.85	0.54	0.32	0.08	No
1.0	10.5	23.3	16.75	-2.49	40.83	1.81	0.54	0.32	0.12	No
1.0	10.5	22.7	17.0	-2.99	40.88	0.23	0.84	2.09	0.10	No
1.0	10.5	23.3	17.0	-2.99	40.89	0.22	0.84	2.09	0.15	No

$500 - 800\mathring{A}$, at most, before breaking sharply down to the X-ray continuum (Stevans et al. 2014). The bolometric luminosity of the accretion flow would only be $L_{\rm bol} = 1{-}2{\times}10^{43}$ergs/s. This liberally assumes a range of X-ray luminosity from negligible to roughly equal to the extrapolated UV continuum. In order to quantify this we note that the central black hole mass is estimated as $M_{bh} \approx 8 \times 10^8 M_\odot$ based on the NICMOS bulge luminosity estimators (Donzelli et al. 2007; Marconi and Hunt 2003). Similarly, gas kinematical estimates find $4 \times 10^8 < M_{bh}/M_\odot < 2 \times 10^9$ (Scharwachter et al. 2013). With this mass estimate, the Eddington rate, $0.00004 < R_{\rm Edd} < 0.0006$, is low compared to low redshift Seyfert 1 galaxies that typically have Eddington rates on the order of a few percent (Sun and Malkan 1989). We want to explore this circumstance in terms of the CLOUDY models, but we need more constraints.

4.4. Redshift of the BEL Region

Table 2 provides a range of BEL distances from the ionization source that are consistent with the weak, soft ionizing continuum and the BEL line ratios and line strengths. We have an extra constraint that arises based on the estimates of M_{bh}. We note that in our fits, the BELs are redshifted relative to the systemic velocity of NGC 1275. However, this redshift is modest, $\sim$ 500km/sec, compared to other high (central black hole) mass broad line objects (Sulentic et al. 2007). Knowing this value to more than a 50% uncertainty is beyond the ability of our methods applied to these weak BELs. The gravitational redshift in terms of velocity and geometrized black hole mass, M, is (Corbin 1997)

$$v_{\rm redshift}/c \approx M/r \ , \quad M \approx \frac{M_{bh}}{10^9 M_\odot} 1.4 \times 10^{14} {\rm cm}. \tag{2}$$

Motional Doppler shifts can be of comparable magnitude, but can only be estimated based on knowing the velocity distribution of the BEL gas and line of sight. These are unknown and their inclusion would be speculative. We note that a pure transverse Doppler shift from transverse Keplerian motion adds a factor of 1.5 to Equation (2) (Corbin 1997). The gravitational redshift can also be partially canceled by an out-flowing BEL gas and there is a strong jet in 3C 84 that can conceivably induce an outflow in the BEL region. All we know is that the gravitational redshift is much lower than the 1000 km/sec - 2000 km/sec redshifts typical of sources with large central black holes and small Eddington ratios (Sulentic et al. 2007). The modest observed BEL redshifts and Equation (2) crudely limits the range of allowable distances from the photo-ionization source to $>\sim 400 - 500M$. We can relate this constraint to the simulations in Table 2

$$\log r > 16.75 \ , \ \frac{M_{bh}}{10^9 M_\odot} = 1 \ , \quad \log r > 16.5 \ , \quad \frac{M_{bh}}{10^9 M_\odot} = 0.5 \tag{3}$$

4.5. Virial Mass Estimates

A related issue are the single epoch virial estimates of M_{bh}. We are proposing that NGC 1275 is similar to the low luminosity sample of (Kaspi et al. 2005), but M_{bh} is clearly much larger than these reverberation sources. So, we explore the virial mass estimators in order to get more restrictions on the location of the BEL region. We cannot use the optical continuum luminosity based estimators since the optical flux is dominated by the synchrotron jet and not the accretion flow emission. Thus, we need to use L(Hβ) as a surrogate for the ionizing continuum. The formula of Greene and Ho (2005); Wu et al. (2003) gives us the type of estimate that we can utilize,

$$\frac{M_{bh}}{M_{\odot}} = 3.6 \times 10^{6} \left[\frac{L(H\beta)}{10^{42}\,\mathrm{erg/s}}\right]^{0.56} \left[\frac{\mathrm{FWHM}}{1000\mathrm{km/s}}\right]^{2} \ . \tag{4}$$

It is very important to note that the reverberation sources at $L(H\beta) < 5 \times 10^{41}$ergs/sec do not correlate strongly with the reverberation radius (Wu et al. 2003; Kaspi et al. 2005). Thus, Equation (4) has much larger uncertainty at the low end of its range than at its high end. Using the results of Table 1 we estimate $\frac{M_{bh}}{M_{\odot}} \approx 1.5 - 3.5 \times 10^{7}$. This is a factor or 10 - 100 less than the estimates in Section 4.3.

In order to understand this discrepancy, we consider the BL-Lac nature of NGC 1275 (Veron 1978). The BL-Lac properties of 3C 84 have been noted in connection with the synchrotron optical emission that hides the accretion generated continuum. The BL-Lac aspect can be very pronounced with optical polarization that changes dramatically in amplitude and position angle, with the largest optical polarization reaching 6% (Angel and Stockman 1980). Such extreme blazar-like properties suggest a small line of sight to the jet axis (Lind and Blandford 1985). We qualify this statement by noting that the evidence does not support extreme BL-Lac behavior. The range of polarization is 1-6 % in Angel and Stockman (1980) and more extensive polarization data [1] covering the time period 2011-2018 indicates an optical polarization that is usually below 2% and extremely rare (2) instances of polarization > 3% were reported. This suggests a slightly off angle BL-Lac. The Hβ BEL is considered to be rotating gas in a flat "pancake-like" region in which the normal to the BEL disk is parallel to the jet axis (Wills and Browne 1986). Thus, the FWHM that appears in Equation (4) depends on the line of sight. For polar lines of sight, Equation (4) will under estimate M_{bh}. In the virial mass estimation,

$$M_{bh} = \frac{R_{\mathrm{BLR}} v_{\mathrm{BLR}}^{2}}{\mathrm{G}} \ , \tag{5}$$

---

[1] from http://www.bu.edu/blazars/VLBAproject.html

where G is the gravitational constant, $R_{\rm BLR}$ is the orbital radius of the BLR (broad line region) and $v_{\rm BLR}$ is the velocity of the BEL gas. In order to relate $v_{\rm BLR}$ to an observed quantity, one defines the de-projection factor, f,

$$v_{\rm BLR} = f{\rm FWHM} \; . \tag{6}$$

Equations (5) and (6) indicate that $M_{bh} \propto f^2$. The de-projection factor has been estimated for various classes of objects that are believed to be differentiated by a line of sight (LOS) (Antonucci 1993; DeCarli et al. 2011). The method of DeCarli et al. (2011) was to estimate M_{bh} from the bulge luminosity of the host galaxy. Using this estimate to set the value of M_{bh} in the virial formula they were able to estimate f for various classes of objects,

$$f_{\rm isotropic} = \frac{\sqrt{3}}{2} \;, \quad f_{\rm quasars} = 2.0 \pm 0.3 \;, \quad f_{\rm blazars} = 5.6 \pm 1.3 \;, \quad f_{\rm BL-Lacs} = 6.9 \pm 2.3 \; . \tag{7}$$

Equation (4) is derived based on assuming an isotropic distribution of BEL gas velocity. Thus, we adopt a correction factor for the estimate in Equation (4) of $(f_{\rm BL-Lacs}/f_{\rm isotropic})^2$ for BL-Lac orientations such as the one that exists in 3C 84. Taking the nominal value of DeCarli et al. (2011) in Equation (7), we expect a correction factor of 64. The orientation corrected central black hole mass estimate based on the data in Table 1 yields $\frac{M_{bh}}{M_\odot} \approx 1.0 - 3.2 \times 10^9$. Alternatively, if we use the blazar correction of 42 associated with the nominal value of $f_{\rm blazars}$ in Equation (7) instead, we get $\frac{M_{bh}}{M_\odot} \approx 0.6 - 1.5 \times 10^9$.

These corrections seem very extreme and we wish to see how they relate to our CLOUDY fits and the redshift constraints on the distance to the BEL region in Equation (3). Assuming a FWHM = 5000 km/s for Hβ from Table 1 and using Equation (5)

$$\log r = 16.75 \;, \; \frac{M_{bh}}{10^9 M_\odot} = 1 \;, \quad f = 3.1 \;, \quad \left[\frac{f}{f_{\rm isotropic}}\right]^2 = 12.8 \tag{8}$$

$$\log r = 16.5 \;, \; \frac{M_{bh}}{10^9 M_\odot} = 0.5 \;, \quad f = 2.9 \;, \quad \left[\frac{f}{f_{\rm isotropic}}\right]^2 = 11.2 \; . \tag{9}$$

Using the line of sight correction factors from Equations (8) and (9) in the virial mass estimator Equation (4) one gets

$$\log r = 16.75 \;, \; \frac{M_{bh}}{10^9 M_\odot} = 1 \;, \quad f = 3.1 \;, \quad \frac{M_{\rm virial}}{M_{bh}} \approx 0.19 - 0.44 \tag{10}$$

$$\log r = 16.5 \;, \; \frac{M_{bh}}{10^9 M_\odot} = 0.5 \;, \quad f = 2.9 \;, \quad \frac{M_{\rm virial}}{M_{bh}} \approx 0.33 - 0.78 \; . \tag{11}$$

Considering the uncertainty in the virial estimate, especially at the low luminosity end, Equations (10) and (11) are within acceptable agreement once the LOS corrections were applied.

4.6. Mitigating the Tension Between Constraints

Equations (1) - (4) combined with Table 2 provide many constraints on the photoionization BEL system.

1. There are the four line ratios in Equation (1).
2. There are the compatible distances from the source in Table 2 that are associated with these ratios in a simple single zone model.
3. There are the constraints on distances from the source based on the line redshifts in Equations (2) and (3).
4. There is the 1-2 order of magnitude under estimate of the central black hole mass from the virial formula in Equation (4).
5. There is the BL-Lac nature of the source, perhaps slightly off angle

The strategy in a complicated system of constraints that are only estimates is to find solutions that fully or partially mitigate the tension between them. We find that this tension is reduced by a slightly off angle blazar correction applied to the virial mass estimate near the minimal allowed distances in the CLOUDY models. The tension can be relieved further with small amounts of intrinsic extinction and possibly low metallicity. We note that if the distance to the BEL is $\log r < 16.75$ low metallicity is required to satisfy the line ratio constraints in Equation (1) based on the CLOUDY simulations. We consider $\log r = 16.75$ to be possibly most viable. It conforms with $Z = 0.1$ and is close to being conforming with $Z = 1.0$ in Table 2. It might be possible to fine tune a solution with $Z = 1.0$ in the over simplified model (especially with some intrinsic extinction). We consider this the best choice for mitigating the tension between constraints based on the following:

1. It is close to reconciling the four line ratios in Equation (1) and the simple single zone CLOUDY model with $Z = 1.0$ within the coarse resolution of Table 2. It does conform with $Z = 0.1$.
2. For $M_{bh} = 10^9 M_\odot$, the gravitational redshift is only 750 km/sec.
3. The f value of 3.1 in equation (8) is intermediate between a quasar and a blazar based on equation (7). Consistent with the modest BL-Lac behavior
4. The line of sight correction reconciles the viral black hole estimate with $M_{bh} \approx 10^9 M_\odot$ within the viral estimators uncertainty.

In summary, the CLOUDY simulations in Table 2 indicate that a BEL region with a number density of $n \sim 1 - 3 \times 10^{10}\,\mathrm{cm}^{-3}$ located $\sim 5 - 10 \times 10^{16}$ cm that is photo-ionized by the thermal emission from an optically thick accretion flow is consistent with the BEL line ratios, the line strengths and the velocity shifts relative to the systemic redshift of 3C84. Furthermore, if the LOS is offset slightly from the normal to planar rotation of the low ionizations lines then the virial mass estimate of M_{bh} conforms with bulge luminosity and kinematic estimates. Integrating this information with the CLOUDY results, we concluded that $r \approx 5 \times 10^{16}$cm is most viable. The mitigation of tension amongst constraints described in this section reinforces the finding that 3C 84 has a BEL region that is photo-ionized by the emission from an optically thick accretion flow similar to the low luminosity Seyfert galaxies in the reverberation sample (Kaspi et al. 2005).

The identification of a BL-Lac type jet within the core of 3C 84 is not a trivial interpretation. The interior jet geometry is far more complex than simple jet models predict (Giovannini 2018). The pc scale structure in terms of jet speed, counter jet to jet flux ratios and free-free absorption strongly indicate a jet orientation much closer to the sky plane than a polar BL-Lac orientation (Walker et al. 2000; Fujita and Nagai 2017). Thus, the interior jet must change orientation, drastically, from a BL-Lac line of sight to an oblique line of sight on very small scales. Possible evidence of this is found in Figure 2 of Giovannini (2018), the inner jet drastically changes direction and morphology ~ 0.1 pc from the core.

4.7. Long Term Time Evolution of the Accretion Flow

We note that the current L_{bol} estimated in Section 4.3 is much lower than would be inferred from [OIII], [OII], and the Mid-IR (in order of increasing distance from the photo-ionizing source). Based on the relative strength of the high ionization lines, the NL region seems to be photo-ionized. From Table 1 we find $L([OIII]\lambda5007)/\mathrm{L}(\mathrm{H}\beta(\mathrm{NL})) \sim 5 - 6$, $\mathrm{L}([\mathrm{OIII}])/\mathrm{L}([\mathrm{OII}]) \approx 2$. L_{bol} can be estimated from $L([OIII])$, $L([OII])$, $\lambda L_{\lambda}(\lambda = 12\mu)$ and $\lambda L_{\lambda}(\lambda = 25\mu)$ (Stern and Laor 2012; Willott et al. 1999; Spinoglio et al. 1995),

$$L_{\mathrm{bol}} = 4000 \left[\frac{L([OIII])}{10^{43}\mathrm{ergs/s}}\right]^{1.39} \left[10^{43}\right] \mathrm{ergs/s}\ , \tag{12}$$

$$L_{\mathrm{bol}} \approx 5000\, L([OII])\ , \tag{13}$$

$$\log[L_{\mathrm{bol}}] = 0.942 \log[\lambda L_{\lambda}(\lambda = 12\mu)] + 3.642\ , \tag{14}$$

$$\log[L_{\mathrm{bol}}] = 0.837 \log[\lambda L_{\lambda}(\lambda = 25\mu)] + 8.263\ . \tag{15}$$

The 12μ (30μ) excess over a synchrotron power law has a luminosity of 1.58×10^{44} erg/s (2.44×10^{44} erg/s) which has been ascribed to dust heated by the AGN (Leipski et al, 2009).

This corresponds to $L_{\rm bol} \approx 2-2\times10^{45}$ergs/s (Spinoglio et al. 1995). For the values of [OIII] and [OII] in Table 1, $L_{\rm bol} \approx 7.1\times10^{44}$ergs/s and $L_{\rm bol} \approx 1.3\times10^{45}$ergs/s, with the bolometric corrections in Stern and Laor (2012); Willott et al. (1999), respectively. Apparently, the accretion flow has decreased in luminosity relative to its value many decades in the past. Presently, $L_{\rm bol}$ is ~ 0.01 of the value imprinted in the surrounding molecular gas. The size of the molecular dust based on subarcsecond Mid-IR imaging is restricted to < 129 pc (Asmus et al. 2014). Thus, the fading of the AGN continuum has likely been occurring on a time frame of many decades to 300 years.

5. The Jet-Accretion Flow Connection

In order to establish a connection between the accretion flow state and the jet power, $Q(t)$, requires the identification of observable quantities that represent $L_{\rm bol}$ and $Q(t)$. In the last section, it was argued that the Hβ BEL luminosity is related to the strength of the ionizing continuum as in other broad line Seyfert galaxies (Gilbert and Peterson 2003). Thus, one of the main goals of this section is to find a surrogate for $Q(t)$,

5.1. A Surrogate for Jet Power

It is far from trivial to find a surrogate for the jet power of a blazar-like jet. Although numerous modeling schemes exist to accomplish this (eg. Ghisellini et al (2010)), the process is highly dependent on the degree of Doppler enhancement of the observed flux density. The Doppler factor, δ, is given in terms of Γ, the Lorentz factor of the outflow; β, the three velocity of the outflow and the angle of propagation to the line of sight, θ; $\delta = 1/[\Gamma(1-\beta\cos\theta)]$ (Lind and Blandford 1985). The Doppler enhancement of the luminosity of an unresolved source is δ^4 and can range from a factor of a ten to a factor of few tens of thousands (Lind and Blandford 1985; Punsly and Tingay 2005). The unresolved source Doppler enhancement is particularly relevant to attempts to model the broadband blazar jet emission. Due to the level of complexity these models are generally reduced to single zone spherical models, the mathematical analog of an unresolved source (Ghisellini et al 2010; Boettcher et al. 2013). One can try to constrain this Doppler factor by making assumptions on the line of sight and the bulk flow of the jet. However, the errors of such methods are also exaggerated by Doppler enhancement, so the method can yield considerable scatter as a result of uncertainty and random fluctuations in the line of sight and Lorentz factor (Punsly and Tingay 2005; Willott et al. 1999). In summary, the flux density is not a reliable method of tracking the intrinsic change in jet power of a blazar jet.

Fortunately, 3C 84 is not typical in this regard. The jet shows order unity changes in mm flux on time scales of weeks as expected for a blazar. This flickering is superimposed on a larger amplitude long term variability time scale of many years to decades (as we show in the data presented in this section). We postulate that the long term background flux variation of the core can be used as a surrogate for $Q(t)$ after the flickering is averaged out. Yet, we do not believe that it can be used to determine $Q(t)$ quantitatively in a reliable manner. We ultimately substantiate this postulate in Section 5.2 (with certain caveats), by revealing evidence that the long term mm flux varies in consort with the ionizing continuum.

The nucleus can be optically thick to synchrotron self absorption (SSA) at wavelengths $\sim$ a few mm based on total flux density measurements (Nesterov et al. 1995). At optically thick frequencies, the flux density is an unreliable surrogate for jet power because it is never clear if one is seeing a change in SSA opacity or luminosity. Thus, one wants to sample the nucleus at high frequency in order to probe optically thin emission that directly relates to the energy release of the jet. Thus motivated, Figure 6 is a plot of the $\approx$ 225 GHz (1.3 mm) flux density over three decades. The 1.3 mm flux density data after 2002 was obtained at the Submillimeter Array (SMA) near the summit of Mauna Kea (Hawaii). 3C 84 is included in an ongoing monitoring program at the SMA to determine the fluxes of compact extragalactic radio sources that can be used as calibrators at mm wavelengths (Gurwell et al. 2007). Observations of available potential calibrators are from time to time observed for 3 to 5 minutes, and the measured source signal strength calibrated against known standards, typically solar system objects (Titan, Uranus, Neptune, or Callisto). The data was downloaded from the Sub-millimeter Array Calibrator archive, http://sma1.sma.hawaii.edu. Before 2002, the data is taken from the literature (Nesterov et al. 1995; Reuter et al. 1997; Trippe et al. 2011). Even though 3C 84 has blazar-like properties, Veron (1978), the 1.3 mm light curve has a predominant background variation on the time scales of many years.

We are looking for a diagnostic of jet activity that is contemporaneous with the Hβ BEL emission. Thus, we want to know the luminosity of the jet as close to the point of origin as possible. Ostensibly, a high frequency like 225 GHz rules out optical thin (steep spectrum) emission and renders the optically thick core the only viable source of flux. Typically, secondary components are optically thin in the mm band and can be ignored at high frequency. But this is not the case during flares in 3C 84. During very luminous flares, the mas scale structure of 3C 84 is very complex due to the extremely luminous secondary components (currently C3) that occur on sub-parsec scales. During the large mm flare in the 1980s, VLBI observations showed that there was more 89 GHz - 100 GHz flux density on mas scales than was detected from the nucleus (Backer et al. 1987; Wright et al. 1988). There is also evidence during the current flare that the secondary, C3, is the major contributor to mm flux density (Hodgson et al. 2018). In order to understand the source of the emission comprising the long term mm wave light curve, we need high resolution images that can segregate the core from the pc scale jet emission. No 1.3 mm VLBI observations exist. However, there is a large history of 43 GHz VLBI observations. The VLBI core flux densities are limited to observations which have a resolution of $\leq 0.55\,\mathrm{mas} \sim 0.6\,\mathrm{lt-yr}$ (Krichbaum et al. 1993; Dhawan et al. 1998; Lister 2001; Suzuki et al. 2012; Nagai et al. 2014; Jorstad et al. 2017). We show these data superimposed on the 1.3 mm light curve in Figure 6 in order to elucidate the connection.

The first 43 GHz VLBI observation that we utilize was based on only 3 stations (Krichbaum et al. 1993). However, amazingly, these researchers were able to obtain an image that closely resembles the morphology of the images from deep 10 station VLBA observations four years later. Thus, we think that this is a credible result. It has the largest restoring beam of our sample, a 0.55 mas circular beam. This raises an issue associated with utilizing a large inhomogeneous sample of archival data. In spite of all of the observations being 43 GHz with VLBA (except the Krichbaum et al. (1993) observation mentioned above) there are different restoring beams in the dozens of observations that we acquired (Dhawan et al. 1998; Lister 2001; Suzuki et al. 2012; Nagai et al. 2014; Jorstad et al. 2017). We are looking for coarse flux variation over time frames of years. Thus, the scatter induced by the inhomogeneous method of rendering the core flux is not a deleterious circumstance, yet it is still prudent to process the core flux densities as uniformly as possible. Most of the observations have a beam size $\approx 0.2\mathrm{mas} \times 0.3\mathrm{mas}$. After 2010.8, the data are obtained from FITS files that were downloaded from VLBA-BU-BLAZAR Program [2]. These data are processed similarly to the Suzuki et al. (2012) in order to maintain a uniform processing method with our main source of observations. This eliminates one potential systematic source of scatter in the core flux density determinations. As with Suzuki et al. (2012), the data is fit with one circular Gaussian for C1 and one circular Gaussian for C3. The source has many small components and is very complicated to fit. As noted in Suzuki et al. (2012), the addition of numerous small components has a negligible effect on the fits to the major components. Our Gaussian fits to C1 consistently have a diameter of $0.13-0.20$ mas and are brighter than the adjacent jet features. There are non-negligible ridges of surface brightness just to the south of the core (Nagai et al. 2014). The implementation of a data reduction technique that results in a small < 0.2 mas circular Gaussian for the core model is an uniform method of segregating the core form these ridges. We expect this to be a robust method of defining the C1 flux density. The lone exception is the 1991 observation of Krichbaum et al. (1993) in which the circular Gaussian diameter is ≈ 0.8 mas. Thus, this data point is likely overestimated relative to the latter estimates. We also added the core peak intensities that were downloaded

---

[2] http://www.bu.edu/blazars

from VLBA-BU-BLAZAR Program [3] to Figure 4. This provides an independent method of interpreting the core luminosity based on the FITS files. One can see a rise from 2010 toward the 2016-2017 flare peak and the subsequent decay in both the total core flux density and the peak intensity.

Figure 6 shows the light curves of both the 43 GHz VLBI core flux density, C(43), and the $\sim$ 225 GHz flux density. The data are selected to cover a time span of $\sim$ 1990 until spring 2017 (a larger data span is shown in Figures 7 and 8). The red and black lines are the third order polynomial fits to C(43) and the 1.3 mm flux density, respectively. The fits help to segregate the long term trends from the superimposed flickering. It is interesting that there is much more dispersion about the 43 GHz core trend compared to the 1.3 mm trend. The two fits are fairly similar from 1991 to 2011. They both show a broad minimum around 1995 -2002, then an upward trend that is very close. The upward trend starts to differ significantly in late 2011 when some abrupt flares start to occur at 1.3 mm. From this time onward, the 1.3 mm light curve shows a significant excess over what is expected from the 43 GHz VLBI observations of the core. There is likely a significant contribution from C3 during the height of flare activity (Hodgson et al. 2018). The flux density of C3 started growing in 2003 and eventually equaled that of the core, C1, in 43 GHz VlBI observations in late 2008 (Suzuki et al. 2012). The very high peak at 1.3 mm in 2015 and 2016 is not indicative of the magnitude of the core flux density. However, C(43) rises from 2011 to 2017 which does seem to mirror the 1.3 mm light curve at least qualitatively. It should be noted that the C(43) light curve does reflect the 2016-2017 peak of the 1.3 mm light curve and the abrupt fading of the 1.3 mm flux density at the end of 2017, so there is definitely a strong causal connection. Our 2017 Copernico observation (see Table 1) occurred during this abrupt decay.

Based on the high level of 1.3 mm flux density relative to the total 43 GHz flux density, Nesterov et al. (1995), and relative to the C1 43 GHz flux density (see Figure 6), there is evidence that significant SSA absorption exists in the nucleus at times. Thus, one must always consider this when interpreting the C1 43 GHz flux density. Thus, if the SSA opacity is significant, we expect a time lag of C(43) relative to changes in the 1.3 mm flux density. We also note that there could very well be large changes in SSA opacity at 43 GHz that might also affect the observed C(43) and this might be the source of the larger scatter from the trend line at 43 GHz compared to 225 GHz.

In summary, during states of low to moderate jet activity, the 1.3 mm light curve agrees with the long term trending of C(43) and is a good surrogate for the luminosity of the jet

---

[3] http://www.bu.edu/blazars

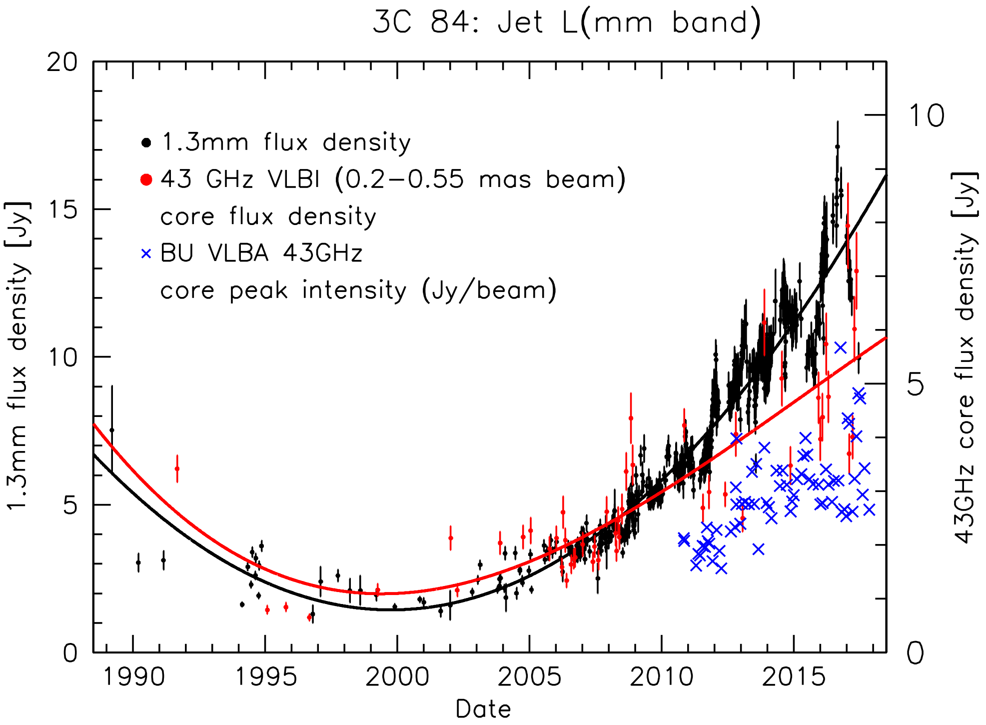

Fig. 6.— A comparison of the 1.3 mm flux density light curve and the 43 GHz VLBI core flux density light curve. The data covers a time span of ∼ 1990 until spring 2017. The black curve and the red curves are the third order polynomial fits to the 1.3 mm and 43 GHz VLBI data, respectively.

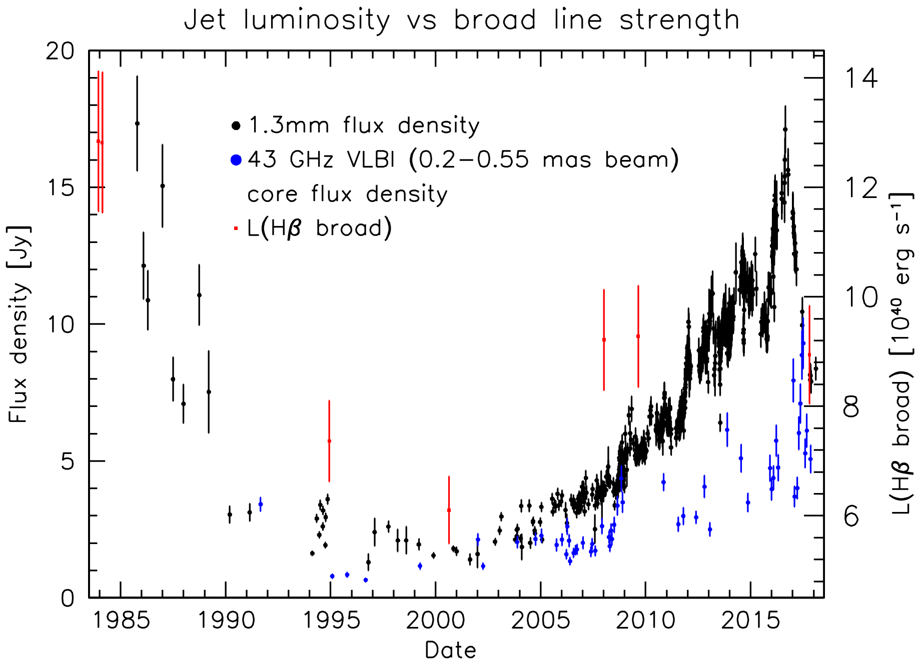

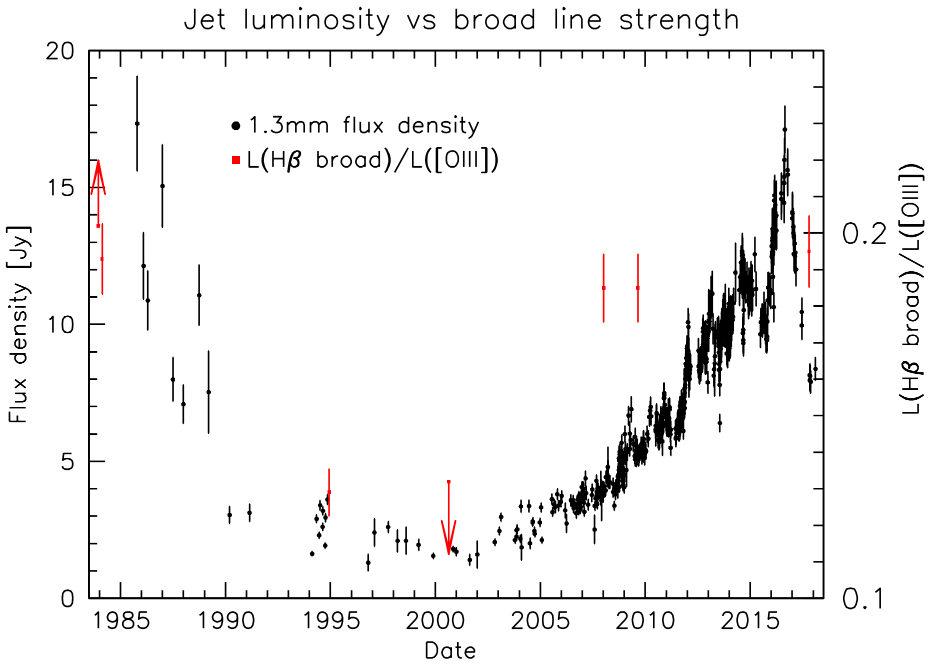

Fig. 7.— The top frame is a plot of the 225 GHz and 43 GHz VLBI core flux densities versus BEL luminosity from Table 1. The bottom frame shows the 225 GHz light curve and the L(Hβ) points from the top frame normalized by L([OIII]λ5007) in a 6 (arcsecond)^2 extraction region.

on the smallest observable scales (~ 0.2 mas). In states of high flare activity, the 1.3 mm light curve will over estimate the luminosity of the jet on the smallest observable scales. The 1.3 mm light curve appears to be a reasonable surrogate for the core luminosity (but, not necessarily $Q(t)$) from the late 1980s to 2012.

5.2. Hβ Broad Line Luminosity and the Luminosity of the Jet Base

The top frame of Figure 7 appears to show a correlation between the L(Hβ) and the luminosity of the base of the jet. The changes in L(Hβ) are modest, so absolute flux calibration is critical. One can use the [OII] or [OIII] NL luminosity as an independent calibration standard, as has been done in reverberation studies (Barth and Bentz 2016). Table 1 shows that the NL luminosity scales with the size of the extraction region. Understanding the effects of the size of the extraction and slit PA on emission line fits was the motivation for our extraction experiments in 2009 and 2017. We need a robust method of normalizing the size of the extraction region if we want to use the NL luminosity as a calibration standard. L([OIII]λ5007) extracted from a region between 1.69" $\times$ 2" $= 3.38\,(\text{arcsecond})^2$ and 2" $\times$ 4" $= 8\,(\text{arcsecond})^2$ can be normalized to a $\approx 6\,(\text{arc second})^2$ extraction region using our 2009 and 2017 extraction experiments in Table 1 (see the bottom frame of Figure 7). The HST 2000.663 observation occurs at the important minimum of jet activity. The large HST [OIII] luminosity relative to the [OIII] luminosity in the smallest (but much larger) extraction regions in 2009 and 2017 indicates that centering losses in the narrow slit were not an issue in the HST observation. The results of our extraction experiment were designed to normalize the extraction region with small changes in the extraction size. As such, we cannot extend this method to the small HST aperture. However, a crude upper limit in Figure 7 is obtained by ignoring the (significant) [OIII] luminosity between 0.2" x 0.2" and our smallest extraction regions of 2" x 2" and 2" x 1.69" [4]. Similarly, the extraction region in 1983.94 is too large to be adjusted with our experiment. We create a lower bound by using our extraction correction from $8\,(\text{arcsecond})^2$ to $\approx (6\,\text{arc second})^2$. The trend in the bottom frame of Figure 7 looks very similar to the trend in the top frame with two independent methods of flux calibration.

If the Hβ BEL gas is photo-ionized by emission from the accretion flow, as seems likely

---

[4] We average the extraction size corrections form the combined 2009 and 2017 results. We average the extrapolation factors from a $3.38\,(\text{arcsecond})^2$ extraction region to a $6\,(\text{arcsecond})^2$ extraction region and from a $4\,(\text{arcsecond})^2$ extraction region to a $6\,(\text{arcsecond})^2$ extraction region. The result is a correction factor of 1.22. This can be used to form a upper limit on L(Hβ)/L([OIII]λ5007) for HST. This is the most stringent upper limit that we can obtain from our experiment.

from the analysis of Section 4, then Figure 7 seems to indicate that the jet luminosity scales with the luminosity of the ionizing continuum and $L_{\rm bol}$. Figure 8 investigates the possibility that long term trends in $F_{225}(t)$ scale with $L_{\rm bol}$. Considering the trends in Figure 6 and the related discussion, it is concluded that the 1.3 mm flux density is a good representation of the core luminosity in low and moderate states of jet activity. Based on 100 GHz VLBI there was still very strong emission in 1987 from the mas scale jet, even though jet activity was decaying (Wright et al. 1988). Thus, the earliest point used to fit the long term trend is 1989.20. The long term fourth order polynomial approximation to the trend, $F_{225}(t)$, is plotted as a blue curve in Figure 8. Based on Figure 6, the last point where the 1.3 mm flux density closely fits the core flux density is chosen to be approximately 2011.87, just before the small 1.3 mm flare. We extended the blue curve 6 years to the left although this is very speculative since it is not being constrained by the data. However, the extrapolation should be fairly accurate around the time of the Palomar observations in late 1983 and early 1994 based on 89 GHz VLBI observations. The core flux density at 89 GHz was 8 Jy in 1983 and 7 Jy in 1984 (Backer et al. 1987). At 1984.0, our extrapolation of the blue curve in Figure 8 is 9.5 Jy at 225 GHz. Thus, the extrapolation gives a reasonable estimate of the core flux density at 225 GHz considering the 89 GHz flux density and the plausible SSA flat spectrum of the core at that time.

The BEL luminosity varies with the strength of the ionizing continuum in each photoionized AGN. This is called the responsivity of the line (Korista and Goad 2004). Empirically, Gilbert and Peterson (2003), find data to support the scalings between BEL luminosity and the UV continuum luminosity, L_{UV},

$$L(H\beta) \propto L_{UV}^{\alpha_H},\ \alpha_H \approx 0.35 - 0.44\ . \tag{16}$$

The orange curve in Figure 8, $L(H\beta)(t)$, is motivated by Equation (16),

$$L(H\beta)(t) = \left[\left[\frac{F_{225}(t)}{1.8\mathrm{Jy}}\right]^{0.4}\right] 6.2 \times 10^{40} \mathrm{ergs/s}\ , \tag{17}$$

where 1.8 Jy is the lowest value of $F_{225}(t)$ in the fourth order polynomial fit in Figure 8 and 0.4 is the approximate exponent, α_H, in Equation (16). The surprisingly good fit combined with Equation (16) and Equation (17) suggests a dynamic in which

$$F_{225}(t) \propto L_{UV}(t)\ . \tag{18}$$

Whether the orange fit is as good as it appears in Figure 8 or not, the figure strongly supports the notion that the causative agent for the long term variation in L(Hβ) and $F_{225}(t)$ is $L_{\rm bol}$. The good fit could be a manifestation of a fortuitous cancelation of systematic errors in our

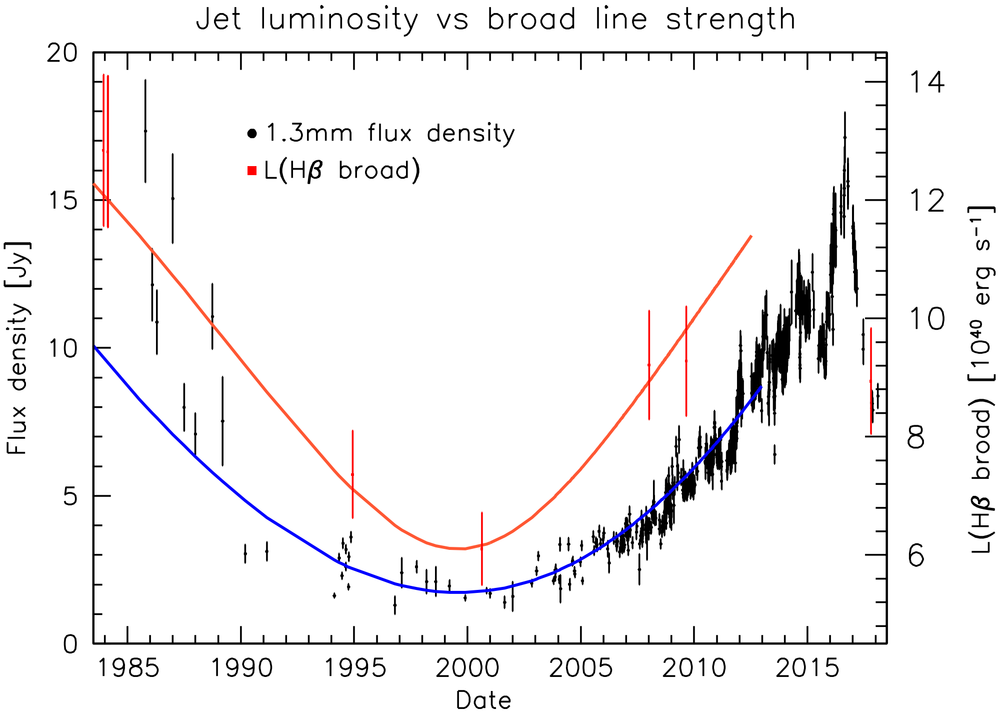

Fig. 8.— The blue curve is a fourth order polynomial fit to the 1.3mm light curve, $F_{225}(t)$. Notice that it underestimates the data before 1988 due the flux from the secondary component during the strong flare. The orange curve is $L(H\beta)(t) = \left[\left[\frac{F_{225}(t)}{1.8\mathrm{Jy}}\right]^{0.4}\right] 6.2 \times 10^{40}$ergs/s. See the text for further discussion. Based on Equation (16), $F_{225}(t)$ scales with the strength of the ionizing continuum.

method. However, given the striking nature of the fit, we feel it should be displayed. The most straightforward physical interpretation of Equation (18) is that $F_{225}(t) \sim Q(t)$ and $Q(t) \sim L_{UV}(t)$. We prefer this interpretation as opposed to assuming that Figures 6 - 8 result from mere coincidence.

The blue trend has one sense of curvature, so there is no way to extend it to the rapid fade in late October 2017 during the Copernico observation. The 1.3 mm flux density was $\approx$ 8 Jy during the Copernico observation, yet L(Hβ) corresponds to a flux density of about 5 Jy during the rise in 2008-2009. The excess can be emission form the strong secondary component C3 (Hodgson et al. 2018). The excess 225 GHz flux density over what was expected from the core luminosity was revealed after mid 2011 in the discussion of Figure 6.

In summary, we presented data that indicated a correlation between L(Hβ) and the luminosity of the base of the jet. The data also supports an interpretation that the connection between the two quantities is an indirect consequence of the fact that accretion power is driving the jet and photo-ionizing the BEL. The implication is that the accretion rate is regulating jet power.

6. Discussion

The notion that a low accretion rate system can produce thermal emission from an optically thick accretion flow and photo-ionize a BEL region has not been anticipated in theoretical works (Novikov and Thorne 1973; Sun and Malkan 1989; Narayan and Yi 1994; Yuan and Narayan 2014). Thus, it is important to critique the robustness or our methods and findings. In this regard, the paper did not disprove other scenarios (besides photo-ionization of virialized gas) for producing the flux in the broad wings of the emission lines. In particular, the collisional excitation and ionization of gas by the jet was not addressed. Utilizing shocks from a jet collision with gaseous clouds has proved a viable method of exciting NL gas in some Seyfert galaxies and radio galaxies (Sutherland et al. 1993; Allen et al. 2008). However, the BEL gas in NGC 1275 has velocities exceeding 3000 km/s in the wings and it is not clear if the scenario can be applied to these high velocities. Before the detailed calculations of Sutherland et al. (1993); Allen et al. (2008) were performed, it was conjectured that the BEL region might be created by a jet interaction with the surrounding medium in radio loud objects (Norman and Miley 1984). This idea has not gained traction primarily because of the development of spectroscopic unification schemes for broad line AGN. Radio loud broad line objects belong to a class of objects known as Population B that are defined by Hβ FWHM $>$ 4000 km/sec. They tend to have low Eddington rates, $R_{\rm Edd} < 0.1$ and include both radio loud and radio quiet objects (Sulentic et al. 2000). Within this population, radio loudness has little or no effect on the BEL profiles (Sulentic et al. 2007). Thus, it has been generally concluded that the same broad emission line mechanism is involved in all broad line objects, regardless of whether there exists a strong jet or no jet. However, one can still question if this is the case in the very extreme ($R_{\rm Edd} \ll 0.1$) Population B source, NGC 1275. Even though this is not a traditional explanation of BEL gas in Seyfert galaxies, it cannot be ruled out due to the very large number of free parameters in the shock/collisional excitation models that cannot be determined by observation. Another item to consider is whether the BEL gas is actually virialized or if it is located within an outflow or inflow. If there is an explanation other than the photo-ionized/virial dynamic indicated in Section 4 then there are three puzzling issues that would need to be explained:

1. The left hand frame of Figure 3 indicates that $L(H\beta)/\lambda L_{\lambda}(1450\mathring{A})$ is typical of what one expects for a low luminosity broad line Seyfert galaxy. If the gas that produces $L(H\beta)$ is not photo-ionized by radiation from the accretion source (as is indicated to be true for the other Seyfert galaxies in the scatter plot based on reverberation studies) then this circumstance is an unexplained coincidence.
2. If the gas that produces the BELs is not photo-ionized by radiation from the accretion source then the fact the CLOUDY photo-ionization models can simulate the line ratios with physically reasonable dimension and density is another coincidence.
3. Consider the red excess in the bottom left had panel of Figure 1 and the BEL fits in Table 1. The wings extend > 3000 km/sec from the line center. What is the mechanism that drives the line emitting, ionized gas at > 3000 km/sec both towards and away from the observer?

Point 3 addresses the location and origin of the high velocity BEL gas. If it is virialized gas within the gravitational potential then points 1) and 2) indicate that it should be photo-ionized by the accretion flow emission. So there would need to be another physical location for the BEL gas, hence the invocation of an outflow or inflow. For outflows, the red excess in the lower left hand panel of Figure 1 is due to an outflow on the far side of the accretion plane. Alternatively, the red excess might be due to emission from an inflow on the near side of the accretion plane. An outflow component to the virialized gas motion is often used to explain BEL regions. However, the outflow is driven by radiation pressure and to achieve gas velocities > 3000 km/sec requires $R_{\rm Edd} > 0.2$, three orders of magnitude larger than what we found for NGC 1275 (Murray et al. 1995). In addition, empirically, BEL outflows manifest themselves as blueshifts in high-ionization lines (e.g., Sulentic et al. 2007; Richards et al. 2011). Evidence of BEL outflows in Hbeta is scant, and mainly associated with sources radiating close to the Eddington limit (Negrete et al. 2018). This is the opposite end of the Eddington ratio distribution than the Eddington ratio of NGC 1275.

Since there is no telescope capable of resolving the BEL gas, one cannot prove categorically that there is not a jet interaction that ionizes BEL emitting outflows or inflows on sub-pc to pc scales. Even so, the scenario is highly challenged because of the "coincidences" 1) and 2) above that would have no explanation. Furthermore, the dynamics of the outflow/inflow at > 3000 km/sec requires an explanation as well.

The other intriguing finding of our analysis was the apparent correlation between the luminosity of the Hβ BEL and the mm band luminosity of the jet base within 0.2 mas of its origin. This is supportive of a dynamic in which both the jet power and the intensity of the photo-ionization field scale with the accretion rate. This is consistent with the magnetically arrested accretion model of radio jet formation (Igumenshchev 2008). In this model, large scale poloidal magnetic flux (define B^P as the poloidal magnetic field component) is transported to the inner region of the accretion flow by the accreting plasma. The inner region of the accretion flow is in rapid (approximately Keplerian) rotation. The magnetic flux is dragged around by the rotating plasma, twisting it azimuthally (creating a toroidal magnetic field B^Φ). The magnetically arrested dynamic also causes the field lines to rotate with a velocity, v^ϕ_F, about the symmetry axis of the central supermassive black hole in the inner accretion flow. To external observers, this creates a poloidal electric field $E_\perp = -(v^\phi_F/c)B^P$, equivalently, a cross-field potential difference. This is tantamount to a poloidal Poynting flux, $S^P = (c/4\pi)B^\phi E_\perp = -(v^\phi_F/4\pi)B^\phi B^P$, flowing outward from the inner accretion disk, parallel to the symmetry axis of the black hole, at the expense of the gravitational potential energy of the plasma. Fully relativistic magnetohydrodynamic simulations show that the efficiency can be extremely large (Poynting flux $\sim 0.4\dot{M}c^2$, where $\dot{M}$ is the accretion rate.) if this occurs very near a rapidly rotating black hole in the active region known as the ergosphere (Punsly et al. 2009).

7. Conclusion

In this article, we described the nature of the weak Hβ BEL in Section 2 (Figure 1 and Table 1). The situation is made clear by the coexistence of a Pα BEL that also arises from transitions from the n=4 state with a similar FWHM as shown in Figure 1 and Table 1.

In Section 3, we found that there is a very weak CIV BEL as well. Section 4.1 showed that the ionizing continuum resembles that of a weak broad line Seyfert galaxy except that the hard ionizing continuum is likely somewhat suppressed (Figure 3). This is consistent with thermal emission from an optically thick accretion flow not an ADAF even though $R_{\rm Edd} \gtrsim 0.0001$. We ran CLOUDY simulations in Section 4.2 that indicated that the weak, soft ionizing continuum provides an explanation of the weak CIV BEL described in Section 3. As a verification of the applicability of these single zone models of the BEL region and ionizing continuum, not only is the small BEL luminosity ratio, L(CIV)/L(Hβ) < 1, replicated, but we also were able to replicate the observed large L(Pα)/L(Hβ) and L(HeIIλ1640)/L(CIV) ratios.

In the process of studying the photo-ionization of the BEL region we uncovered some other interesting aspects of the accretion flow. In Sections 4.4-4.6, we found that the virial mass estimates combined with our CLOUDY simulations indicate that the low ionization BEL region is being viewed near the polar axis. Combining this with the optical polarization properties, we concluded that the innermost jet (within 0.1 pc from the source) is best interpreted as a slightly off angle BL-Lac jet. In Section 4.7, evidence was also shown that $L_{\rm bol}$ has been fading over decades or centuries. We point out that NGC 1275 is not the only known LLAGN with a CIV BEL. NGC 4579 is a LLAGN, with both high ionization and low ionization BELs (Barth et al. 2001).

The simplified single zone CLOUDY analysis was considered in the context of the BL-Lac nature of the nucleus and line of sight effects in the the virial mass estimates. We conclude that the explanation of all of these results, in consort, favors the following model of the BEL gas: a density of $\sim 1-3\times 10^{10}{\rm cm}^{-3}$ located at a distance of $\sim 5\times 10^{16}$cm from the photo-ionizing source, with approximately solar metallicity.

Section 5 presented data showing that $L(H\beta)$ correlates with the luminosity of the jet less than 3 light months (0.2 mas) from the central engine. We explored the implications to the dynamics of jet formation. It appears that accretion power is driving the jet and photo-ionizing the BEL. This was interpreted in terms of magnetically dominated accretion models in Section 6.

Based on the potential theoretical importance of this connection between the accretion flow and the jet power, it would be of significant scientific value to monitor $H\beta$ and $P\alpha$ every two or three weeks. The 225 Ghz luminosity is monitored regularly and 43 GHz VLBA observations occur monthly. A "reverberation mapping" of the jet and BELs might provide more information on the location of the line emitting gas relative to jet base.

We would like to thank Ski Antonucci and Patrick Ogle for discussions and insight into the nature of the ionizing continuum. Kirk Korista also shared his knowledge of photo-ionization of broad emission line clouds. We thank Barbara Balmaverde for sharing the details of the data reduction of the Chandra X-ray data. Jeffrey Hodgson also shared his extensive VLBI knowledge of this source, for which we are thankful. This study makes use of 43 GHz VLBA data from the VLBA-BU Blazar Monitoring Program VLBA-BU-BLAZAR funded by NASA through the Fermi Guest Investigator Program [5]. The VLBA is an instrument of the Long Baseline Observatory. The Long Baseline Observatory is a facility of the National Science Foundation operated by Associated Universities, Inc. The results are based in part on observations collected at Copernico telescope (Asiago, Italy) of the INAF - Osservatorio Astronomico di Padova. Data was published with permission of the Submillimeter Array Calibrator website http://sma1.sma.hawaii.edu/callist/callist.html. The Submillimeter Array is a joint project between the Smithsonian Astrophysical Observatory and the Academia Sinica Institute of Astronomy and Astrophysics and is funded by the Smithsonian Institution and the Academia Sinica.

REFERENCES

Abdo, A. A., Ackermann, M., Ajello, M., et al. 2010, ApJ, 720, 912

Allen, M. G., Groves, B. A., Dopita, M. A., Sutherland, R. S., Kewley, L. J. 2008, ApJS, 178, 20

Angel, J. and Stockman, H. 1980, ARA&A 18, 321

Antonucci, R.J. 1993, Annu. Rev. Astron. Astrophys. 31 473

Asmus, D., Honig, S., Gandhi, P., Smette, A., Duschl, W. 2014, MNRAS, 439, 1648

Backer, D., Wright, M., Plambeck, R. et al. 1987, ApJ, 322, 74

Barvainis, R. 1987, ApJ, 320, 537

Balmaverde B., Capetti A., Grandi P., 2006, A&A, 451, 35

Balmaverde, B. and Capetti, A. 2014 A&A 563 119

Barth, A., Ho, L., Filippenko, A., Rix, H.-W., Sargent, W. 2001 ApJ, 546 205

Barth, A., Bentz, M. 2016 MNRAS Lett, 458, 109

Boettcher, M., Reimer, A., Sweeney, K. and Prakash, A. 2013 ApJ 768 54

Boroson, T. A., and Green, R. F. 1992, ApJS, 80, 109

---

[5] http://www.bu.edu/blazars/VLBAproject.html

Buttiglione, S., Capetti, A., Celotti, A., et al. 2009, A& A, 495, 1033

Buttiglione, S., Capetti, A., Celotti, A., et al. 2010, A& A, 509, 6

Cardelli, J., Clayton, G., Mathis, J. 1989 ApJ 345 245

Corbin, M. 1997, ApJ 485 517

Chuvaev, K. 1985, PAZh 111 803

DeCarli, R., Dotti, M., Treves, A. 2011, MNRAS 413 39

Dhawan, V., Kellermann, K. I., Romney, J. D. 1998, ApJL, 498, 111

Donzelli, C., Chiaberge, M., Macchetto, F. D.; Madrid, J. P.; Capetti, A.; Marchesini, D. 2007 ApJ 667 780

Dimitrijevic, M. S.; Popovic, L. C.; Kovacevic, J.; Dacic, M.; Ilic, D. 2007 MNRAS 6374 118

Evans, I. and Koratkar 2004, ApJS 150 73

Ferland, G., Porter, R., van Hoof, P. et al. 2013 Revista Mexicana de Astronoma y Astrofsica 49 137

Filippenko, A., and Sargent, W. 1985, ApJS, 57, 503

Fujita, Y. and Nagai, H. 2017, MNRAS, 465, L94L98

Gammie, C. F., Narayan, R., Blandford, R. 1999, ApJ, 516, 177

Ghisellini, G., Tavecchio, F., Foschini, L., Ghirlanda, G., Maraschi, L., Celotti, A. 2010 MNRAS 402 497

Giovannini, G.; Savolainen, T.; Orienti, M. et al. 2018, Nature Astronomy https://doi.org/10.1038/s41550-018-0431-2

Gilbert, K., Peterson, B. M. 2003, ApJ, 587, 123

Greene, J. E., & Ho, L. C. 2005, ApJ, 630, 122

Gurwell, M. A., Peck, A. B., Hostler, S. R., Darrah, M. R., & Katz, C. A.2007 in *From Z-Machines to ALMA: (Sub)Millimeter Spectroscopy of Galaxies* Astronomical Society of the Paci?c Conference Series, 375, 234.

Hardcastle, M., Evans, D. and Croston, J. 2009, MNRAS, 396, 1929

Ho, L. C., Filippenko, A., and Sargent, W. 1995, ApJS, 98, 477

Ho, L. C., Filippenko, A., and Sargent, W. 1997, ApJS, 112, 315

Hodgson, J., Rani, B., Lee, S.-S. et al. 2018, MNRAS 475 368

Humason, M. 1932, PASP, 44, 381

Igumenshchev, I. V. 2008 ApJ 677 317

Jarvis, M., McLure, R. 2006 MNRAS 369 182

Jorstad, S., Marscher, A., Morozova, D., et al. 2007, ApJ, 846, 98

Kaspi, S., Maoz, D., Netzer, H., et al. 2005, ApJ, 629, 61

Khachikian, E., Weedman, D. 1974 ApJ 192 581

Kishimoto, M., Honig, S. F., Beckert, T., Weigelt, G. 2007, A&A, 476, 713

Korista, K. T., Baldwin, J., Ferland, G., Verner, D. 1997, ApJS, 108, 401

Korista, K., Goad, M. 2004, ApJ, 606, 749

Krichbaum, T., witzel. A., Graham, D. et al. 1983 A & A 275 375

Laor, A., Fiore, F., Elvis, M., Wilkes, B. J.,McDowell, J. C. 1997, ApJ, 477, 93

Lawrence, C. et al. 1996, ApJS 107 541

Leipski, C., Antonucci, R., Ogle, P., Whysong, D., 2009 ApJ, 701, 891

Lind, K., Blandford, R.1985 ApJ 295 358

Lister, M. L. 2001, ApJ, 562, 208 541

Mahadevan, R. 1997, ApJ 477, 585

Marconi, A., Hunt, L.K. 2003, ApJL, 589, 21

Marziani, P., Sulentic, J., Dultzin-Hacyan, D., Calvani, M., Moles, M. 1996, ApJS 104 37

Marziani, P., Sulentic, J., Stirpe, G., Zamfir, S., Calvani, M. 2009, A&A 495 83

Mathews W. G., Ferland G. J., 1987, ApJ, 323, 456

Norman, C., Miley¡ G. 1984, A & A, 141, 85

Murray, N. et al 1995, ApJ 451 498

Nagai, H., Haga, T., Giovannini, G., et al. 2014, ApJ, 785, 53

Narayan R., Yi I., 1994, ApJL, 428, 13

Negrete, C, Dultzin, D., Marziani P. , Esparza, D. , Sulentic, J. et al. 2018 2018arXiv180908310N

Nesterov, N., Lyuty, V., Valtaoja, E. 1995, A & A 296 638

Novikov, I. and Thorne, K. 1973, in *Black Holes: Les Astres Occlus*, eds. C. de Witt and B. de Witt (Gordon and Breach, New York), 344

Punsly, B., Tingay, S. 2005 ApJL 633 89

Punsly, B., Igumenshchev, I. V., Hirose, S. 2009 ApJ 704 1065

Quataert, E., Di Matteo, T., Narayan, R., Ho, L.C. 1999 ApJL 525 89

Reuter, H.-P., Kramer, C., Sievers, A., et al. 1997, A & ASS, 122, 271

Reynolds, C., Punsly, B. and O'Dea, C. P. 2013, ApJL, 773, 10

Richards, G,, Kruczek, N., Gallagher, S., Hall, P., Hewett, P., 2011, AJ, 141, 167

Riffel, R., Rodriguez-Ardila, A., Pastoriza, M. G., 2006, A&A, 457, 61

Rosenblatt, E., Malkan, M., Sargent, W.; Readhead, A. 1994, ApJS 93 73

Ruff, A., Floyd, D., Webster, R.; Korista, K.; Landt, H. 2012 ApJ 754 18

Scharwachter, J., McGregor, P. J., Dopita, M. A., Beck, T. L. 2013 MNRAS 429, 2315

Seyfert, C. 1943, ApJ 97 28

Son, D., Woo, J.K., Kim, S. 2012, ApJ 757 140

Spinoglio, L., Malkan, M. A., Rush, B., Carrasco, L., Recillas-Cruz, E. 1995, ApJ, 453, 616

Stern. J. and Laor, A. 2012 MNRAS 426 2703

Stevans, M., Shull, M., Danforth, C., Tilton, E. 2014 ApJ 794 75

Sulentic, J., Marziani, P., and Dultzin-Hacyan, D. 2000 ARA& A 38, 521

Sulentic, J., Bachev, R., Marziani,P., Negrete, C. A., Dultzin, D. 2007 ApJ 666 757

Sutherland, R., Bicknell, G., Dopita, M. 1993 ApJ 414 510

Sun, W.-H., and Malkan, M. A 1989, ApJ 346 68

Suzuki, K., Nagai, H., Kino, M., et al. 2012, ApJ, 746, 140

Trippe, S., Krips, M., Pietu, V., et al. 2011, A & A, 533, 97

Veron, P. 1978, Nature 272 430

Walker R. C., Dhawan V., Romney J. D., Kellermann K. I., Vermeulen R. C., 2000, ApJ, 530, 233

Willott, C., Rawlings, S., Blundell, K., Lacy, M. 1999, MNRAS 309 1017

Wills, B., Brotherton, M 1995, ApJL 448 81

Wills, B.J., Browne, I.W.A. 1986 ApJ 302 56

Wright, M,, Backer, D., carlstrom, J. et al 1988 ApJL 329 61

Wu, X.-B., Wang, R., Kong, M. Z., Liu, F. K., Han, J. L. 2004, A&A, 424, 793

Yuan F., Narayan R., 2014, ARA & A, 52, 529

This preprint was prepared with the AAS LATEX macros v5.2.